THE JOURNAL OF PHYSICAL CHEMISTRY C

C: Surfaces, Interfaces, Porous Materials, and Catalysis

Stability of Adsorbed Water on TiO-TiN Interfaces. A First Principles and Ab Initio Thermodynamics Investigation

Jose Julio Gutierrez Moreno, Marco Fronzi, Pierre Lovera, Alan O'Riordan, and Michael Nolan

J. Phys. Chem. C, **Just Accepted Manuscript** • DOI: 10.1021/acs.jpcc.8b03520 • Publication Date (Web): 11 Jun 2018

Stability of Adsorbed Water on TiO_2-TiN Interfaces. A First Principles and Ab Initio Thermodynamics Investigation

*José Julio Gutiérrez Moreno[1], Marco Fronzi[2], Pierre Lovera[1], Alan O'Riordan[1], Michael Nolan[1]**

[1]Tyndall National Institute, University College Cork. Lee Maltings, Dyke Parade. Cork, T12 R5CP, Ireland.
[2]International Research Centre for Renewable Energy, State Key Laboratory of Multiphase Flow in Power Engineering, Xi'an Jiaotong University, Xi'an 710049, Shaanxi, China.

michael.nolan@tyndall.ie

Abstract

Titanium Nitride (TiN) surfaces can oxidise and the growth of a TiO_x layer on the surface along with the likely presence of water in the surrounding environment can modify the properties of this widely used coating material. The present Density Functional Theory study, including Hubbard +U correction (DFT+U), investigates the stability of adsorbed water at TiO_2-TiN interfaces with different defects, that serve as a model for an oxide layer grown on a TiN surface. Surface free energy calculations show the stability of perfect TiN-TiO_2 interface at regular O pressures, while oxygen vacancy-rich $TiO_{1.88}$–TiN is more favourable at reducing conditions. An isolated water is preferentially adsorbed dissociatively at perfect and oxygen defective interfaces while molecular adsorption is more stable at higher coverages. The adsorption energy is stronger at the oxygen defective interfaces which arises from the high concentration of reduced Ti^{3+} and strong interfacial atomic relaxations. Ab initio atomistic thermodynamics show that water will be present at high coverage on TiO_2-TiN interfaces at ambient conditions and the pristine interface is only stable at very low pressure of O and H_2O. The results of these DFT+U simulations are important for the fundamental understanding of wettability of interfacial systems involving metal oxides.

1. Introduction

Titanium nitride (TiN) is a widely used coating material with multiple applications[1-4] and is used as a conducting layer or to enhance the hardness, resistance to corrosion and biocompatibility of different materials.[3-6] The TiN surface can oxidise at high temperatures or after long exposure times at regular ambient conditions.[7-13] The formation of a Ti-based oxide (TiO_x) layer on the nitride surface tends to reduce the adherence of the coating. This results in a deterioration of the resistivity, mechanical properties or anti-corrosion features of TiN.[13-15] In different applications, the substitutional doping of N into the crystalline TiO_2 matrix can introduce N 2p states above the O 2p valence band, reducing the large TiO_2 bandgap.[16] Thus the controlled growth of TiO_2 on TiN may be used for tuning the TiO_2 optical bandgap by nitride formation leading to an optimized catalytic performance under visible light.[16-18]

The oxidation of TiN is a complex reaction. When oxidation takes place at high temperature, a void-free stoichiometric ordered TiO_2 crystalline structure can form on the TiN surface. In contrast at low temperatures, defects such as vacancies or TiN_xO_y transition structures can form during growth and are prone to remain trapped in the interface.[11, 19] When the oxidation takes place at regular atmospheric conditions the TiO_x structure is expected to show features of either rutile or anatase. The oxidation of (100)-oriented TiN leads to the formation of a rutile TiO_2 (110) out-of-plane orientation in which a lattice mismatch of up to 8.69% is possible.[11] In a previous publication,[20] we have found that rutile (110)–TiN is a stable interface system in which new Ti-O bonds form in the interface region. Defects such as Ti vacancies in TiN, O vacancies in TiO_2 or interdiffusion of O and N atoms within the interface may be present as a result of the growth process and must be taken into account in interface models. Our density functional theory (DFT) study of the rutile TiO_2 (110)–TiN (100) interface model system, including a Hubbard +U correction on Ti 3d states, showed the presence of reduced Ti^{3+} ions in TiO_2. The Ti^{3+} cations are formed as a result of charge transfer from the nitride to the oxide after interface formation and can also originate in the

non-stoichiometric systems from the introduction of O vacancies. The Ti^{3+} cations are preferentially localized near the interface region. The TiO_2 Electronic Density of States (EDOS) shows localised Ti^{3+} defect states forming in the mid-gap between the top edge of the valence band and the bottom of the conduction band.

Rutile TiO_2 is one of the most extensively investigated metal oxides and (110) is the most stable rutile TiO_2 crystal face. TiO_2 applications cover a broad range of fields such as photocatalysis, sensing, corrosion protection or biocompatible coatings for medical implants.[21-28] TiO_2 has the capacity to oxidise organic molecules, therefore environmental photocatalytic catalysts containing TiO_2 can be used for applications such as decomposition of pollutants or water oxidation.[26, 29, 30] Titanium alloys are used for biomedical applications while their enhanced biocompatibility is attributed to the oxide film that forms on its surface.[22, 31, 32] In addition, the wettability of TiO_2 can be tuned by surface morphology modifications or UV irradiation enhancing the hydrophilic features of the surface for its use as antibiofouling or self-cleaning coating material.[33-36] The multitude of TiO_2 applications and the fact that water is present in almost every environment, either in gas or liquid phase, explains the great interest in and necessity for studying the interaction of water with different TiO_2 surfaces.[21, 27, 37-40] However, despite the great deal of work carried out in the last two decades[21, 27, 37-40], there still remains some controversy regarding the details of water adsorption at TiO_2 surfaces such as rutile (110). Water adsorption can be described either as molecular or dissociative; [38, 41] surface hydroxyls are produced upon dissociative adsorption. Most experimental works agree that water adsorbs molecularly at a pristine rutile (110) surface while dissociation may take place on site defects and step edges.[21, 38, 42] On the other hand, the outcomes from most theoretical studies on water adsorption at TiO_2 over the last twenty years are still unclear and the adsorption of water can be highly dependent on the

simulation setup parameters, i.e. surface coverage, slab thickness or exchange-correlation functional.[21]

Kowalski et al.[43] carried out the most complete DFT study on water adsorption on rutile (110) to date. They found that an isolated water molecule has a preference for dissociation while molecular adsorption is more stable at higher surface coverages. The energy differences between molecular and dissociative adsorption modes at partially covered surfaces with more than one H_2O are very small. Based on these results, the authors thus suggest the likely formation of molecular H_2O islands where the molecules at the boundary may dissociate. Despite significant studies on TiN thin films carried out in the last four decades,[5, 10, 44-47] more fundamental works aiming to understand the oxidation of TiN and the interactions between water and both the TiN surface and oxidised TiN interface are lacking. Actually, there are very few examples of first principles computational works on water adsorption at oxide-metal interfacial systems in general. These are important as the structure and stability of the metal substrate -oxide interface can strongly modify the characteristics and activity of the surface, with water adsorption a prototype of such an effect. A fine example is that of supported ultra-thin MgO, specific examples being single layer MgO-Ag[48, 49] or MgO-Mo.[50] On these systems, thin layers of MgO show strong water adsorption compared to the extended (100) MgO surface. In addition, the barrier for water dissociation can be significantly lowered. The only available DFT study for water adsorption on the TiN (200) surface reported weak adsorption energies, in a range between -0.19 and -0.33 eV per molecule.[51] Whereas as far as we are aware, there are no theoretical publications on water adsorption at TiO_2-TiN interfaces. Therefore, given the importance of water interactions at metal-oxides interfaces and how it may modify the characteristics of an oxide, this work presents a detailed first principles analysis to obtain a deeper understanding of the water adsorption process at the TiO_2-TiN interface. We use several TiO_2 rutile (110)-TiN (100) interfaces that serve as model systems

for oxidised TiN. Rutile TiO_2 (110) and TiN (100) surfaces have the lowest surface energy for their respective polymorphs and compositions.[52, 53] Our models were described in detail in Ref.[20] and involve a stoichiometric rutile (110)-TiN (100), with a lattice mismatch of only 2.7% along $[1\bar{1}0]$ and 4.6% in the [001] direction with respect to TiN (100). In addition, we further consider off-stoichiometric systems with up to 100% O vacancies in the interface and structures in which O and N are exchanged within the interface.

We apply Hubbard-Corrected Density Functional Theory (DFT+U) calculations to consistently describe partial reduction of Ti atoms in TiO_2 that form from charge transfer between TiN and TiO_2 or after the creation of O vacancies.[20] We then discuss the molecular and dissociative adsorption of water on the different interfaces as a function of the surface coverage. Finally we go beyond total energy calculations and use ab initio atomistic thermodynamics[54] to analyse the thermodynamic stability of the water-oxide-nitride system at different temperatures within a range of oxygen and water pressure conditions.

With these simulations, we aim to describe the influence that oxide-nitride interfaces, the inclusion of interface vacancies and the presence of reduced Ti^{3+} will have on the stability and coverage of water at oxidised TiN. The simulations presented herein provide a comprehensive insight into the structural and electronic properties of oxidized TiN in a realistic hydrated environment, which will play a critical role for several key properties of this system including water dissociation or the adhesion of biomolecules at the surface.

2. Computational Details

We perform Density Functional Theory (DFT) calculations within 3-dimensional periodic boundary conditions with the Vienna Ab Initio Simulation Package (VASP).[55] The projector augmented-wave (PAW) potentials[56, 57] are used to describe the core-valence interaction, where the valence electrons (H $1s^1$ electrons, Ti $4s^2$ and $3d^2$ electrons, N $2s^2$ and $2p^3$ electrons and O $2s^2$ and $2p^4$ electrons) are described by periodic plane waves with a cut-off energy of

400 eV and the remaining electrons are considered as core states. The generalized gradient approximation in the form given by Perdew and Wang (GGA-PW91)[58] was employed for the approximate exchange correlation functional. Self-consistency in the energy is reached when successive energy differences are less than 10^{-4} eV while the atomic relaxation is stopped when all the forces are less than 0.02 eV/Å.

We should note that the incomplete cancellation of the exchange term in the DFT GGA exchange-correlation functionals typically results in an inconsistent delocalisation of the partially filled d and f states in reducible and rare earth metal oxides, including TiO_2.[59, 60] To overcome this drawback, the DFT+U method defines a screened on-site Coulomb interaction which penalizes the delocalization of the Ti 3d states.[61] Thus, we perform DFT+U corrected calculations, with U = 4.5 eV applied on the Ti 3d electrons in TiO_2, to account for the potential reduction of Ti atoms that can form in the TiO_2-TiN interface. The U value was chosen based in previous works on charge localization in TiO_2-TiN interfaces[20] and defective TiO_2.[59, 62-64] We use Bader charge analysis[65] to further assess the localization of reduced Ti cations.

We calculated the equilibrium lattice for the bulk TiN (a = 4.26 Å) and rutile TiO_2 (a = 4.64 Å; c = 2.97 Å) using a Monkhorst-Pack sampling grid of (14 x 14 x 14) k-points and (4 x 4 x 4) k-points respectively. Rutile TiO_2 (110) and TiN (100) are the most stable low index crystal cuts for rutile TiO_2[21] and TiN.[46, 66] Upon cleaving from the bulk, the 5-layer thick (10.66 Å) rock-salt TiN (100) surface is composed of neutral planes with TiN stoichiometry and the 4 O–Ti–O tri-layer (11.10 Å) TiO_2 slab exhibits a rutile (110) surface structure. A vacuum thickness of 15 Å was introduced between the interface slabs to avoid interactions along the surface normal. The TiN (100) supercell slab has 120 atoms and lattice dimensions a = 8.51 Å; b = 12.77 Å. The stoichiometric rutile TiO_2 (110) surface contains 144 atoms and has lattice dimensions a = 8.92 Å; b = 13.12 Å. We use a (4x4x1) Monkhorst-Pack sampling

grid and Methfessel-Paxton smearing function with σ = 0.1 eV to integrate the Brillouin Zone. In addition to the perfect TiO_2-TiN stoichiometric system, we also evaluated interface structures in which several O bridging atoms were removed from the interface and a configuration in which we exchanged O and N atoms within the interface. More information about the construction of these interfaces are given in a previous publication.[20] The relaxed structures of the interface models along with the relevant input and output files are available via open-access online repository.[67] The vacancy formation energy is given by the difference between the energy of the ideal system and the sum of the energy of the defective system plus half of the total energy of an O_2 molecule. The relative energy of the O/N exchanged structure was calculated with respect to the ideal interface structure. The interfacial binding energy is given by the difference in energy between a TiO_2 and a TiN free-standing slabs and the total energy of the TiO_2-TiN interface.

The adsorption of water was simulated by the DFT relaxation of H_2O molecules or hydroxyls at different adsorption sites on rutile (110) with different interface structures. We simulated coverages of 1/6 mono-layer (ML), 1/2 (ML) and 1 ML water on rutile (110). For the high coverage interface models, the water molecules or hydroxyls were all simultaneously adsorbed taking the bare surface as initial structure. The adsorption energies (E_{ads}) per adsorbed water were computed for molecular and dissociative adsorption modes using the following expression:

$$E_{ads} = (E_{hydrated} - E_{surf} - n \cdot E_{H_2O})/n \quad (1)$$

Where E_{surf} and $E_{hydrated}$ are the total energy of the system before and after the adsorption of water respectively. The energy of an isolated water molecule was calculated using a Γ-point sampling grid and the same plane wave cut-off and convergence criteria as the slabs. The energy of a single water molecule is multiplied by the number of waters in the system (n).

Van der Waals corrections can be included in water adsorption studies. Previous work on water adsorption at TiO_2 surfaces show that van der Waals (vdW) corrections stabilize water adsorption by 0.13 eV for a single H_2O on anatase (001)[68] and by 0.1 eV for a single H_2O on rutile (110).[69] An stabilisation of 0.18 eV is seen for water adsorption on CeO_2 (111).[70] However, given the large adsorption energies that we find for water on TiO_2-TiN interfaces, such changes in the computed adsorption energy are not significant enough to change any of our key results and we therefore do not include any vdW corrections.

To analyze the thermodynamic stability of the different interface models when exposed to a given environment, we use the DFT-derived total energies as input into an atomistic thermodynamics framework, which considers the effect of the surrounding gas phase as a reservoir that is in thermodynamic equilibrium with the surface. Assuming that the gas reservoir exchanges particles with the system without affecting its chemical potential, the interface energy can be calculated as follows:

$$\gamma(p,T) = 1/A[G - \sum N_i \mu_i(p,T)] \quad (2)$$

where, A is the interface area, G is the Gibbs free energy of the crystal, $\mu_i\ (p,T)$ is the chemical potential of the atomic species in the system and the term N_i is the total number of atoms of species i. We assume that the interface is in equilibrium with an environment formed from a mixture of two different chemical species in the gas-phase, namely O_2 and H_2O, which are considered to be in non-equilibrium with each other. This assumption allows us to treat the chemical potential of water and oxygen as independent variables, so that a broad spectrum of environmental conditions can be treated.

Equation 2 can be rewritten to separate the contributions to the energy of bulk TiN and TiO_2 from the contribution of the two independent chemical potentials (μ_O and μ_{H2O}):

$$\gamma(p,T) = 1/A[G - N_{TiN} g_{TiN} - N_{TiO_2} g_{TiO_2} - (N_O - 2N_{Ti})\mu_O - N_{H_2O}\mu_{H_2O}] \quad (3)$$

where g_{TiN} and g_{TiO2} are the calculated bulk energies of TiN and TiO_2 per formula unit considering their lattice parameter at the interface. Here, the chemical potential of water can be considered as resulting from the separate contributions of the hydrogen and oxygen.

Approximating water vapor and oxygen as ideal gases, we explicitly introduce pressure and temperature in our model through the analytic relation between chemical potentials and the temperature and pressure of the two gas reservoirs as follows:

$$\mu_O(p,T) = \left[\frac{1}{2}E_{O_2} + \mu'_{O_2} + k_B T ln\left(\frac{p_{O_2}}{P^0}\right)\right] \quad (4)$$

$$\mu_{H_2O}(p,T) = \left[E_{H_2O} + \mu'_{H_2O} + k_B T ln(\frac{p_{H_2O}}{P^0})\right] \quad (5)$$

Here, T and p represent the temperature and partial pressure of the two gases, p^0 denotes atmospheric pressure and k_B is the Boltzman constant. μ' is the energetic term that includes contributions from rotations and vibrations of the molecule, as well as the ideal-gas entropy at 1 atm which can be calculated or taken from experimental values listed in thermodynamic tables.[71] In the following we will measure the chemical potentials with respect to the calculated energy of the isolated molecules, and therefore define the relative chemical potentials of species i to be $\Delta\mu_i(p,T) = \mu_i(p,T) - E_i$. A more detailed description of the methodology used here can be found elsewhere.[72-74]

3. Results

3.1. Oxidised TiN model surfaces (TiO_2-TiN interfaces)

We now briefly summarise our results on TiO_2 (110)–TiN (100) interfaces; a detailed discussion is presented in a previous publication.[20] The TiO_2 (110)–TiN (100) interface structure was prepared from interfacing surfaces cleaved from a rutile ($P4_2/mnm$) TiO_2 structure with lattice constants $a = b = 4.64$ Å and $c = 2.97$ Å and a cubic rock-salt TiN

($Fm\bar{3}m$) with lattice a = 4.26 Å. Both values are in good agreement with the experimental lattice parameters.[75, 76] The rutile TiO_2 (110) structure has two types of oxygens on the surface: the three-fold coordinated (O_{3f}) and the under-coordinated two-fold oxygen (O_{2f}) bridging two surface Ti atoms. There are also two kinds of Ti on the surface: the five-fold coordinated (Ti_{5f}) and the six-fold coordinated (Ti_{6f}) which is bridged by two bridging O_{2f} and these alternate along the [001] direction. The rutile (110) (3x2) surface supercell, with equilibrium lattice constants a = 8.91 Å; b = 13.12 Å, was compressed 2.7% along $[1\bar{1}0]$ and 4.6% along [001] to match the TiN (100) (2x3) surface supercell equilibrium lattice of a = 8.51 Å; b = 12.77 Å. The compressed rutile unit cell was then placed on the TiN surface, assuming that in our approach the oxide grows on the TiN and thus it has to adjust to the substrate structure.

The formation of defects such as O vacancies[77] or the interfusion of N and O atoms[11] within the interface is common during TiO_x growth on the TiN surface and can affect the properties of the system. Therefore in addition to the ideal TiO_2–TiN interface, we increased the complexity in our models by introducing several non-stoichiometric or non-ideal structures. The interface models used in this work shown in Figure 1 include:

a) Stoichiometric and defect-free (perfect) TiO_2 (110)–TiN (100) interface.

b) Non-stoichiometric oxygen defective interfaces, in which several bridging interfacial O_{2f} atoms were removed from the perfect system. For this paper, there are two different cases:

b.1) interface with 3 O vacancies, which forms a non-stoichiometric $TiO_{1.94}$–TiN interface system.

b.2) interface with 6 O vacancies, in which all of the bridging O_{2f} atoms have been removed from the interface, forming a $TiO_{1.88}$–TiN interface system.

c) O/N exchanged interface, in which one oxygen atom from TiO_2 and a nitrogen atom from TiN exchange their positions in an otherwise perfect interface.

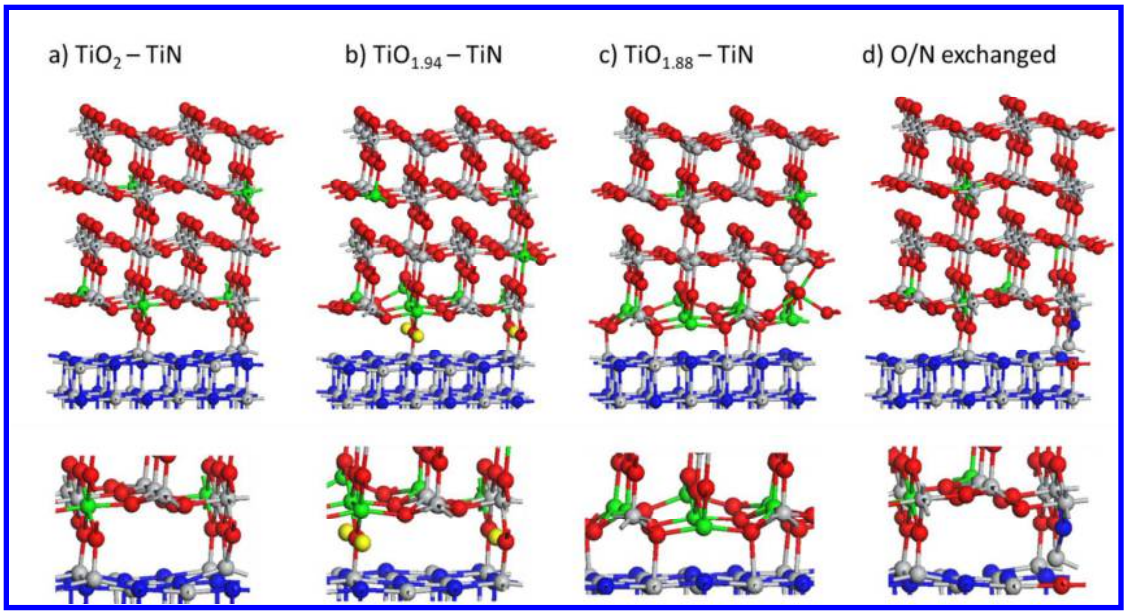

Figure 1. Rutile TiO_2 (110)–TiN (100) interface models: a) ideal interface, b) O-defective $TiO_{1.94}$–TiN interface, c) O-defective $TiO_{1.88}$–TiN interface and d) O/N exchanged interface. Zoom of the interfacial regions are shown underneath. Ti^{3+} atoms in TiO_2 are green, Ti^{4+} atoms in TiO_2 and all Ti in TiN are grey, N atoms are blue, O atoms are red, and the yellow spheres represents the vacancy sites in (b). The top panels show the oxide surface and interface region and the bottom panels show a zoom of the interface region.

The O vacancy and interface formation energy values are listed in Table 1. Figure 2 shows the interface energy as a function of the chemical potential ($\Delta\mu_0$) for our TiO_x-TiN interfaces. We observe strong adhesion of the deposited oxide on TiN due in part to the small lattice mismatch and also to the formation of strong Ti-O bonds in the interface.[20] The perfect interface, which is stable for values of $\Delta\mu_O > -3.15$ eV, presents an $E_{bind} = -5.27$ eV; or -1.32 eV per site for the four interfacial Ti–O binding sites. The non-stoichiometric $TiO_{1.88}$–TiN has the most favourable interface energy for reducing conditions with $\Delta\mu_O < -3.15$ eV and exhibits strong interfacial bonding with $E_{bind} = -4.39$ eV, or -0.88 eV per biding site. Figure 2 shows that the $TiO_{1.94}$–TiN interface is energetically unfavoured compared to the other models. This is consistent with our previous work, where was found that despite the high energy needed for the formation of one O vacancy at the perfect interface, the further

introduction of vacancies in an O-defective system progressively becomes more favourable, leading to the stability of highly non-stoichiometric interfaces.[20] Despite its thermodynamic instability, the differences between the $TiO_{1.94}$–TiN surface energy compared to more favourable interfaces for $\mu_O \sim -3.36$ eV is quite small, thus defects may form from an initially perfect interface under certain conditions. However the most expected cause of defect formation is likely to be during oxide growth and the defects may then be kinetically trapped in the interface after the TiO_x processing of TiN and affect the structure and electronic properties of the system. Therefore we will also describe the $TiO_{1.94}$–TiN in the following sections to ensure the completeness of our study.

The exchange of O and N in the interface region is only 0.82 eV higher relative to the perfect interface. Figure 2 shows that the interface energy of the O/N exchanged interface is only ~0.01 eV/Å^2 higher in energy than the perfect interface while both lines are parallel upon variation of μ_O due to the same O composition in both systems.

Table 1. Formation energy for different non-stoichiometric structures evaluated on the rutile TiO_2 (110)–TiN (100) interface region. The different interfacial systems are listed in the first column. Column 2 presents the O vacancy formation energy of the TiO_{2-x}-TiN interfaces and energy difference between the O/N exchanged interface with respect to the ideal system. Column 3 presents the total interfacial binding energy of the ideal and O-defective systems and column 4 presents the interfacial binding energy normalized by the number of Ti-O bonds in the interface.

	E_{defect} *(eV/atom)*	$E_{binding}$ (eV)	$E_{binding}$ (eV/site)
TiO_2 – TiN	-	-5.27	-1.32
$TiO_{1.94}$ – TiN	1.79	-4.77	-1.59
$TiO_{1.88}$ – TiN	1.30	-4.39	-0.88
O/N exchanged	0.82	-	-

Upon formation of the interface, the TiO_2 inter-layer distances are shortened in the outermost and in the interfacial regions. The larger separation between the layers in the bulk-like region results in the absence of some Ti–O (bonds are plotted when the Ti–O distance is less than 2.30 Å). Ti atoms on the TiN surface layer migrate from their initial positions on the surface to bind with O in the perfect, $TiO_{1.94}$–TiN and O/N exchanged systems. We do not observe significant distortion of the atoms under the TiN surface.

We use Bader charge analysis to identify the presence of reduced Ti^{3+} ions in the oxide. We find Bader charges of *ca.* 1.30 electrons on the Ti^{4+} atoms in TiO_2 while reduced Ti^{3+} cations exhibit typical Bader charges of *ca*. 1.65 electrons and spin magnetizations with absolute values between 0.8-0.9 μ_B. The charge transfer from TiN to rutile (110) forms reduced Ti^{3+} cations, which are primarily localised next to the interface. In the off-stoichiometric defective systems, more Ti^{3+} cations are formed in the system due to the extra electrons introduced after the creation of vacancies. The formation of reduced Ti, perhaps also influenced by the compression applied to compensate the lattice mismatch between TiO_2 and TiN, leads to a rotation of the TiO_2 octahedra perpendicular to the [001] axis. The larger size of Ti^{3+} compared to Ti^{4+} introduces a strong distortion in the rutile structure leading to the formation

of amorphous-like domains particularly in the interfacial region of the off-stoichiometric interfaces.

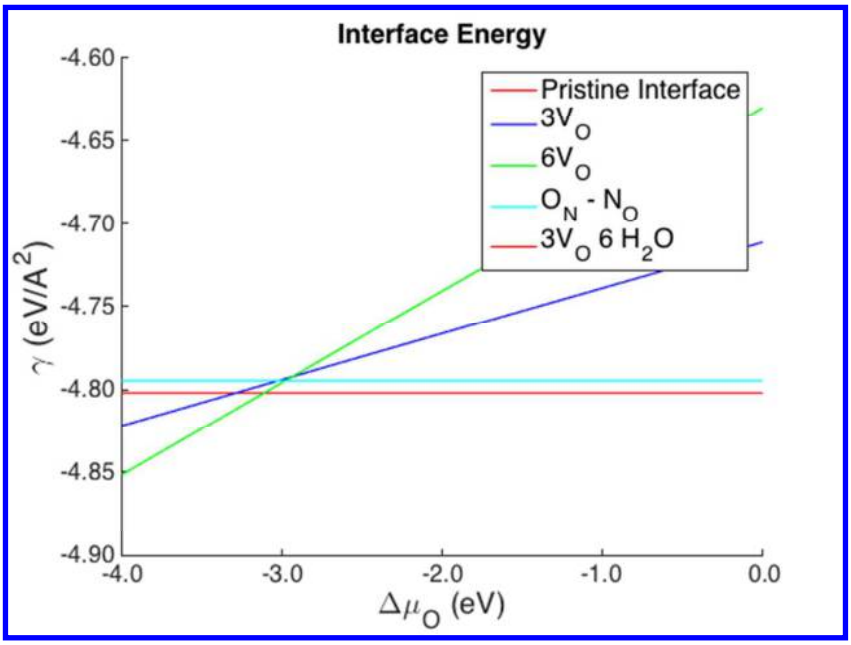

Figure 2. Interface energy (γ) as a function of the chemical potential of oxygen ($\Delta\mu_0$) as defined in the methodology section. The negative values of μ_0 correspond to reducing atmospheric conditions. The γ of TiO_2- TiN (pristine interface) is represented by a red line, the $TiO_{1.94}$- TiN interface ($3V_O$) is represented in blue, the $TiO_{1.88}$- TiN interface ($6V_O$) is represented in green and the O/N exchanged interface in cyan.

3.2 Water adsorption at TiO_2-TiN

Water can be found in almost any environment, either in gas or liquid phase, and can modify the characteristics of the material with which interacts as well as impact on hydrophilicity/phobicity or solvate molecules near the surface. Thus it is important to understand how the presence of water can modify the structure and electronic properties of an oxidised TiN surface when it is present in the surrounding environment. In this study, we simulate the adsorption of water in molecular (H_2O) and dissociated (OH-H) adsorption modes at perfect, O-defective TiO_{2-x}–TiN and O/N exchanged interfaces. The H_2O molecules are adsorbed at the exposed rutile (110) surface in the most favourable adsorption site[21],

which is on top of a surface Ti_{5f} coordinated atom. For the dissociated water model (hydroxylated surface), an OH is adsorbed on an undercoordinated surface Ti_{5f} site and the remaining H from each water is transferred to an adjacent bridging O_{2f} site.[21] We discuss the stability of the molecular versus dissociated adsorption mode as a function of the surface coverage and the nature of the TiO_2–TiN interface. Our supercells have up to six surface Ti_{5f} sites available for water adsorption, thus we tested surface coverage ratios of 1/6 water mono-layer (1/6 ML) (1 H_2O molecule), 1/2 ML (3 H_2O molecules) and 1 ML (6 H_2O molecules). **Table 2** presents the computed adsorption energy per water molecule for molecular and dissociated water adsorption at TiO_2-TiN, $TiO_{1.94}$-TiN, $TiO_{1.88}$-TiN and O/N exchanged interfaces as a function of the water surface coverage. A graphical representation of the change in water adsorption energy as a function of coverage is shown in **Figure 3**, in which the energy values for molecular adsorption are linked with solid lines and energy values for the dissociated adsorption mode are linked with dashed lines.

The relaxed atomic structures of the molecular and dissociative adsorption modes of water on the rutile (110) surface in TiO_2-TiN interfaces are shown in **Figure 4** and **Figure 5**, with the different interfaces distributed in rows and the water surface coverage in columns. Figures showing the water adsorption structures that include the TiO_2-TiN interfacial region are presented in the Supporting Information, Figures S2 and S3.

The negative energy values in Figure 3 indicate the favourable adsorption of water at all oxide-nitride interfaces. The dissociative adsorption mode is more stable at 1/6 ML coverage at perfect and oxygen defective interfaces. These results are in line with a previous theoretical study by Kowalski el at.[43] that found preferred dissociative adsorption for single isolated water molecules at rutile (110). In addition, our computed binding energies for an isolated water molecule are stronger that those reported in the literature for rutile (110) surfaces; these lie in a range between -0.76 eV and -0.93 eV for molecular adsorption and between -0.66 eV

and -1.04 eV for dissociative adsorption, depending on the computational set-up.[43, 78] Our results show in addition that adsorption energy of the isolated OH-H is significantly stronger at the oxygen defective interfaces compared to the stoichiometric models. The TiO_2-TiN interface thus promotes water adsorption when compared with pure rutile (110) and this is as a result of the presence of the reduced Ti^{3+} sites present when the oxide forms an interface with TiN.

Table 2. Computed adsorption energy ($E_{adsorption}$) per water molecule adsorbed at different TiO_x (110)–TiN (100) interfaces. The energy values for the molecular adsorption mode of water (mol) are and for dissociative adsorption (diss) are represented in the columns. The rows give the adsorption energy values as a function of the water surface coverage

	$E_{adsorption}$ / water molecule (eV)							
	TiO_2-TiN		$TiO_{1.94}$-TiN		$TiO_{1.88}$-TiN		O/N exchanged	
Coverage	mol	diss	mol	diss	mol	diss	mol	diss
1/6	-1.14	-1.48	-1.85	-2.04	-1.58	-5.08	-0.82	-0.75
1/2	-1.03	-0.92	-1.18	-1.75	-2.76	-1.17	-0.93	-0.81
1	-1.01	-0.94	-1.03	-1.05	-1.08	-0.86	-0.91	-0.73

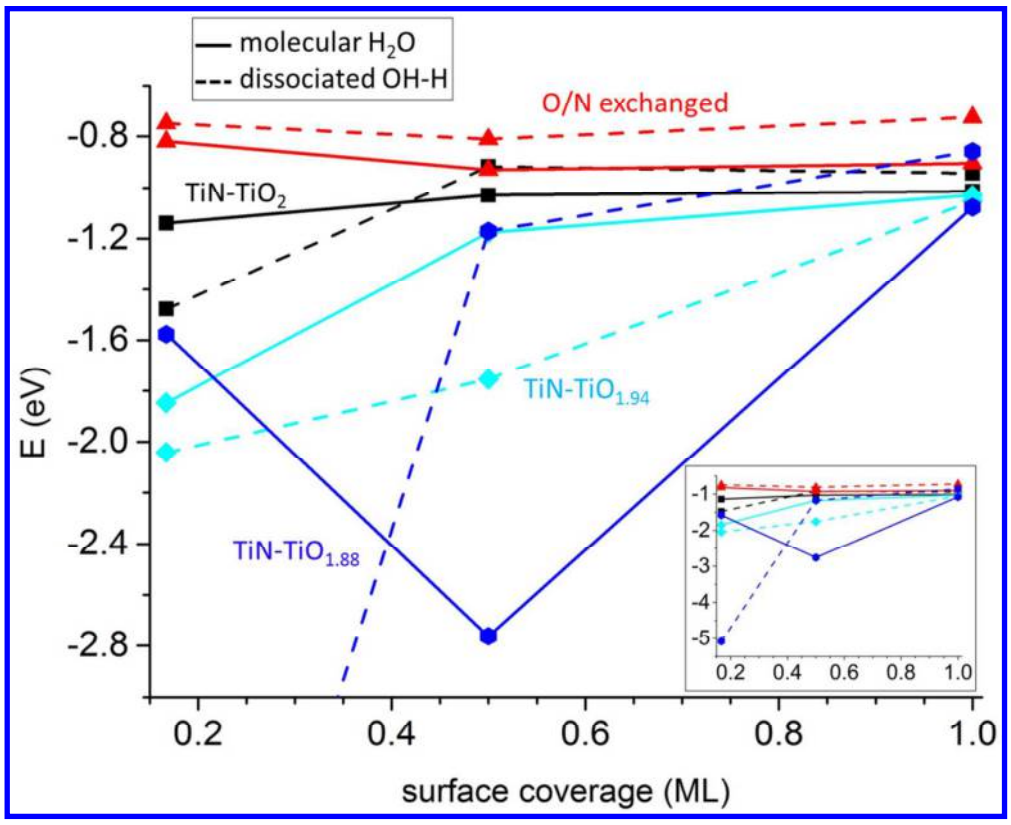

Figure 3. Adsorption energy (E) per water as a function of the water coverage. The energy values for the molecular adsorption mode of water are linked with solid lines while and those for dissociative adsorption are linked with dashed lines to guide the eye. The different interfaces are represented with different colours and labelled in the figure. The inset shows energy values in a range between -0.5 eV and -5-5 eV, units are the same as in the main graph.

The stronger adsorption energy for dissociated water at 1/6 ML coverage, particularly on the highly oxygen defective surfaces may be related in part to the higher concentration of reduced Ti^{3+} in TiO_2 while it can also be influenced by TiO_{2-x}-TiN interfacial atomic relaxations. This would be consistent with the preference for dissociative adsorption of water on defective rutile (110) with surface O vacancies[42, 79, 80]. However, we do note that in the latter studies this is a mechanism in which the OH group fills the vacancies and a hydroxyl is formed with bridging oxygen on the surface. On other metal oxide surfaces, the presence of O vacancy sites, e.g. CeO_2[81, 82], Cu_2O[83] or Al_2O_3[83] also promotes water dissociation. In particular, a DFT+U study on defective CeO_2(111) found that dissociative water adsorption

was more favourable than molecular adsorption by up to 1.15 eV at CeO_{2-x} (111) with one oxygen vacancy and by 0.27 eV on a Ni-doped surface.[82] Both systems have reduced Ce^{3+} present so that reduced metal cations appear to promote water dissociation on metal oxides. In addition, experiments showed the hydroxyl concentration on reduced $CeO_{1.7}$ (100) to be 1.6 times larger than at stoichiometric CeO_2 (100).[83]

However, on moving to higher coverages, molecular adsorption is the most stable at higher coverages of half and one monolayer water for the perfect, O/N exchanged and $TiO_{1.88}$-TiN interfaces so that the apparent role of Ti^{3+} on water dissociation is now diminished. We suggest therefore that the interface relaxations promote water adsorption in general and surface relaxations can be more easily accommodated at low coverages which may promote dissociative water adsorption.

In investigating high water coverages, we compare two different distributions of water at 1/2 ML coverage on the rutile surface at the perfect and O/N exchanged interfaces. The **aligned distribution** adsorption mode, in which three H_2O molecules are adsorbed at the same rutile [100] row is 0.06 eV/molecule more favourable than **a non-aligned distribution** in which H_2O molecules are adsorbed on alternate undercoordinated surface Ti sites on different [100] rows. The preference for the aligned distribution is due to the H bonds that are formed between adjacent water molecules and is in agreement with previous publications on water adsorption at TiO_2 rutile (110).[43] The difference in stability between the water distributions at 1/2 ML coverage is much larger on the $TiO_{1.88}$-TiN, where the aligned distribution leads to a binding energy of -2.76 eV/molecule, which is more stable by 1.31 eV/molecule compared to the non-aligned distribution of water.

The adsorption energy is usually used to estimate the strength of the bonds created between the adsorbed water molecules or hydroxyls and the rutile surface. However the total

adsorption energy is also determined by the contribution of atomic relaxations in the TiO_2-TiN interface after water is adsorbed. Therefore to obtain deeper insights into the origin of the high adsorption energies calculated in some interfaces, i.e. $TiO_{1.88}$-TiN covered with 1/2 ML of H_2O, it is important to estimate the contribution of the interface relaxation to the total binding energy. To estimate this contribution, we remove three water molecules from the 1/2 ML covered surface and perform a DFT+U relaxation of $TiO_{1.88}$-TiN. The interface relaxation is then given by the difference in energy between the pristine surface, before water adsorption, and the interface relaxed after the water desorption. The $TiO_{1.88}$-TiN interface with 1/2 ML of aligned H_2O exhibits an adsorption energy that is strongly influenced by the interfacial atomic relaxations, which is responsible for -1.86 eV out of the total computed adsorption energy of -2.76 eV. In fact, the half-covered $TiO_{1.88}$-TiN interface (Figure 4) exhibits a strongly disordered TiO_2 structure within the interfacial region that forms after the adsorption of water on the rutile surface. In this interfacial amorphous-like region some Ti atoms occupy an interstitial-like position within the rutile structure. The distorted rutile structure in the highly reduced model is influenced by the large concentration Ti^{3+} cations in the interface, with larger atomic radii compared to Ti^{4+}.

Molecular water tends to become more stable when adsorbed on the rutile surface at higher surface coverages. Molecular adsorption is more stable at perfect, O/N exchanged and $TiO_{1.88}$-TiN interfaces while at $TiO_{1.94}$-TiN interface the molecular and mixed models are degenerate in energy. The small difference in energy between the molecular and dissociative adsorption, also found in other theoretical studies,[43, 84, 85] suggests that the rutile (110) surface in TiO_2-TiN which will be covered by molecular water aligned in rows distributed along [100], where some hydroxyls may form at certain atmospheric external conditions.

Our computed energies per water molecule for a water monolayer at TiO_2-TiN interfaces range between -0.91 eV on O/N exchanged interface and -1.08 eV on $TiO_{1.88}$-TiN, which are

consistent with those reported in the literature for full water coverage on rutile (110), which lie in a range between -0.8 eV and -1.0 eV.[43, 84, 85] The adsorption energy is stronger for the systems with larger concentration of reduced Ti^{3+}. The stability of molecular water at high surface coverage might be due the H-bonds formed by the H_2O molecules aligned along the rutile [001] direction on the rutile (100) surface. The binding energy per water is stronger when isolated than on fully covered surfaces, which is also found for the rutile (110) surface.[43] Counterintuitively, we may expect that the formation of H bonds on highly covered surfaces will lead us to a more stable system. Nevertheless, the energy gain due to the H-bonds formation is balanced by the energy required to drive the surface relaxations, leading to very strong binding energy values in which we should however be aware of the different contributions of each component to the total energy.[43]

Temperature programmed desorption spectroscopy (TPD) experiments on water at rutile (110) detected a desorption peak at around 270-275 K, which is assigned to the desorption of water from 5-fold coordinated Ti on the TiO_2 surface.[86-88] The estimated desorption energy values for water adsorbed at 5-fold coordinated Ti were found to go from 0.74 eV to 0.64 eV with increasing coverage, which is consistent with adsorption energies computed from DFT. The cited TPD experiments present weaker water adsorption on rutile (110) compared to our predicted binding energy for water at TiN-TiO_2 interfaces, most likely as a result of the presence of Ti^{3+} species in TiO_2 as discussed above. The decrease in desorption energy with increasing surface coverage found from TPD is also consistent with t weakening of water adsorption at high coverage found in our DFT calculations.

If we begin with a fully covered hydroxylated surface, the relaxation results in spontaneous formation of H_2O molecules on the perfect, O/N exchanged and $TiO_{1.94}$-TiN surfaces, which indicate the instability of a high coverage of dissociated water on these interfaces. Although hydroxyls does not recombine on $TiO_{1.88}$-TiN, the difference in energy between the two

adsorption modes is the largest (0.22 eV) among all the interfaces under study. The strong and negative adsorption energy values and the spontaneous formation of H_2O molecules after relaxation suggest the formation of surfaces that may become fully covered by a layer of molecular water after long exposure times. It has been observed that a high concentration of reduced Ti^{3+} induced by UV illumination of TiO_2 increases the concentration of hydroxyls and therefore enhances the hydrophilicity of the surface.[89] Our models show the fully hydroxylated surfaces to be more stable at oxygen defective interfaces, which contain a larger amount of Ti^{3+} cations than the stoichiometric interfaces. Therefore the formation of molecular H_2O from OH-H recombination at hydroxylated TiO_2 surfaces may be related to the conversion from hydrophilic to hydrophobic observed upon oxidation of TiO_2 surfaces.[89]

Looking at the individual interfaces, we observe that the adsorption of molecular water is always more favourable at the O/N exchanged compared to surface hydroxylation, although the computed adsorption energy is not significantly dependent on the surface coverage. However the small energy differences, up to *ca.* 0.2 eV, suggest the possible formation of a mixed layer of hydroxyls along with water molecules at higher water coverages. The dissociative adsorption of water is more favourable than molecular for 1/6 ML coverage at the perfect and O defective systems. At the ideal interface, an isolated water is strongly adsorbed in dissociative mode with E_{ads} = -1.48 eV. At higher coverages of water, molecular adsorption becomes more favourable. The lower binding energy for surface coverage ≥ 1/2 ML suggest the predominant stability of H_2O molecules, while the small energy difference may allow the coexistence with some hydroxyls on the surface for certain conditions, as will be discussed in the next section.

In the $TiO_{1.88}$-TiN interface, a single OH-H seems to be strongly adsorbed, decreasing the overall energy of the system by 5.08 eV. We found that the adsorption energy of a single dissociated water molecule includes a significant contribution arising from interface

relaxation ($E_{surf\text{-}relax}$ = -1.17 eV); this still results in a rather strong surface-water binding energy of -3.91 eV. The $TiO_{1.94}$-TiN interface shows a preference for dissociative adsorption at all surface coverages, which is quite strong at partially covered surfaces. The water adsorption energy for the fully hydroxylated $TiO_{1.94}$-TiN surfaces is very close in energy to molecular adsorption with a difference of only 0.02 eV. Closer inspection shows that upon relaxation 4 H_2O molecules form when starting from the initially hydroxylated surface. Although mixed adsorption is favourable on fully covered $TiO_{1.94}$-TiN, we showed previously that this interface is less stable than a stoichiometric or a highly non-stoichiometric interface like $TiO_{1.88}$-TiN. The $TiO_{1.94}$-TiN interface also presents a strong binding energy of -2.76 eV/molecule at half-covered surface, while in this case the relaxations caused by the added molecule contribute 1.86 eV to the calculated adsorption energy. This significant contribution leads to an adsorption of energy of 0.90 eV/molecule between the distorted surface and the water molecules.

Table 3. Bond distances (expressed in Å) between O from adsorbed water and surface Ti atoms and H, after adsorption on rutile TiO_2 (110) – TiN (100) interfaces. Molecular (mol) and dissociated (diss) adsorption modes with increasing surface coverage are distributed in lines. The ideal, $TiO_{1.94}$–TiN, $TiO_{1.88}$–TiN and O/N exchanged interfaces are represented in columns. Top-down listed distances represent adsorption sites between 1 and 6 respectively, when applicable. For the H atoms, the top half values correspond to the distances between "H_a" and its nearest O and the second half correspond to the distances measured from atom "H_b". The atom site labels are shown in the inset figure under the table.

	Bond Distances (Å)							
	TiO_2-TiN		$TiO_{1.94}$-TiN		$TiO_{1.88}$-TiN		O/N exchanged	
Coverage	Ti-O	O-H	Ti-O	O-H	Ti-O	O-H	Ti-O	O-H
1/6 (mol)	2.16	0.97	2.16	0.97	2.19	0.97	2.18	0.97
		1.03		1.03		1.02		1.02
1/6 (diss)	1.85	0.97	1.90	0.97	1.89	0.97	1.91	0.97
		0.99		0.99		0.99		1.00
1/2 (mol)	2.26	0.98	2.23	0.98	2.28	0.98	2.26	0.98

	2.26	0.98	2.24	0.98	2.26	0.99	2.25	0.99
	2.25	0.98	2.23	0.98	2.28	0.99	2.25	0.99
		1.03		1.04		1.03		1.03
		1.03		1.03		1.03		1.03
		1.03		1.04		1.03		1.03
1/2 (diss)	1.95	0.99	2.07	0.97	2.02	0.97	2.05	0.97
	1.85	1.01	1.93	1.00	1.90	1.00	2.16	1.01
	1.87	0.98	1.89	0.97	1.89	0.97	1.90	0.97
		0.97		1.05		1.01		1.03
		0.98		1.04		1.00		1.03
		0.98		1.05		1.01		0.99
1 (mol)	2.26	0.98	2.25	0.98	2.27	0.99	2.27	0.98
	2.26	0.98	2.26	0.98	2.25	0.99	2.27	0.98
	2.26	0.98	2.25	0.99	2.30	0.98	2.26	0.99
	2.30	0.98	2.28	0.99	2.28	0.98	2.29	0.99
	2.30	0.98	2.28	0.99	2.30	0.98	2.29	0.98
	2.31	0.98	2.28	0.98	2.26	0.99	2.30	0.98
		1.03		1.04		1.03		1.03
		1.03		1.04		1.03		1.03
		1.03		1.04		1.03		1.03
		1.02		1.03		1.03		1.03
		1.02		1.03		1.03		1.03
		1.02		1.03		1.03		1.03
1 (diss)	2.02	0.98	2.23	1.00	1.99	0.99	2.23	1.00
	2.00	0.98	2.05	0.98	1.92	0.98	2.01	0.98
	2.23	0.99	2.23	0.99	2.00	0.98	1.97	0.98
	2.25	0.99	2.05	0.98	2.02	0.98	2.02	0.99
	2.26	0.99	2.26	1.00	1.89	0.99	1.99	0.98
	2.26	0.99	2.26	0.99	2.01	0.99	1.98	0.99
		1.03		1.03		1.05		1.02
		1.02		1.05		0.97		1.02
		1.02		1.03		1.03		1.02
		1.03		1.04		1.05		1.06
		1.03		1.02		0.98		1.02

1.03 1.02 1.03 1.02

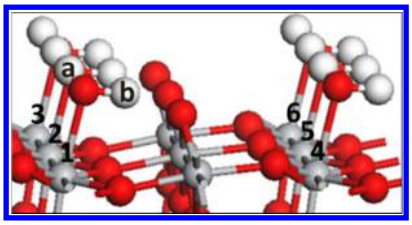

The interatomic distances between O atoms from adsorbed water molecule or hydroxyls and Ti sites in the surface together with the distances between H atoms from water and the nearest oxygen sites are listed on Table 3. The Ti-O distances between surface Ti and O from water increase upon increasing coverage of water, which is consistent with a general weakening of water adsorption energies.

For the models with adsorbed molecular water, the Ti-O distances for oxygen of the isolated water and the surface Ti range between 2.16-2.19 Å at 1/6 ML, between 2.23-2.26 Å at 1/2ML coverage and between 2.26-2.31 Å at 1ML coverage. The increasing Ti-O distance to oxygen of water along with the decreasing adsorption energy per adsorbed water at higher water coverages indicates the progressive saturation of the surface; this is also affected by surface relaxations on rutile (110).

On the hydroxylated surface, the Ti-O distances in Ti-OH species are shorter than the corresponding Ti-O distances in $Ti\text{-}OH_2$ for molecularly adsorbed water. Computed Ti-O distances in Ti-OH are between 1.85-1.91 Å for an isolated molecule, between 1.85-2.16 Å at 1/2ML and between 1.89-2.26 Å at 1ML coverage.

As mentioned before, the formation of hydrogen bonds between neighboring water molecules is important for the stabilization of molecular water along the [100] rows on rutile, especially on fully covered surfaces. Distances between H_a (H atoms located over surface five-fold coordinated Ti – see inset of Table 3) and O from neighboring water range between 1.98-2.04 Å on the covered surface. In addition, we measure distances between 1.53-1.57 Å from H_b

(see Table 3 inset) to surface two-fold coordinated O, both of which can contribute to the stabilization of the molecular water rows.

Surface Ti_{5f} atoms migrate after binding with O on the partially covered surfaces. The migration of surface Ti is larger at surfaces covered by dissociated water, where this adsorption mode is more favourable than the molecular for 1/6 ML coverage. On the perfect surface, the surface Ti migrates outwards by 1.20 Å with respect to the undercoordinated Ti on the same rutile [100] row (water row) and between 1.10-1.19 Å with respect to the atoms on the empty row (bare row). On $TiO_{1.94}$-TiN, the migration of Ti is 1.08 Å with respect to the undercoordinated Ti on the water row and 1.03-1.10 Å with respect to the atoms on the bare row. At the $TiO_{1.88}$-TiN interface, surface Ti migrates 1.18 Å along [110] with respect to the atoms on the water row and between 1.00-1.05 Å with respect to the atoms on the bare row. The effect of the adsorbed OH-H is extended though the subsurface and affects the TiO_2 layers near TiN, introducing an apparent disorder in the rutile structure at the interfacial region. The surface relaxation introduces an important contribution to the calculated total adsorption energies, as previously discussed. At the O/N exchanged, the surface Ti migrate between 0.99-1.03 Å with respect to the Ti on the same [100] row and 0.92 Å with respect to the bare row when the water molecule is dissociated.

The adsorption of an isolated water molecule on the O/N exchanged interface results in Ti migration of Ti_{5f} by 0.25 Å as measured from the Ti atoms on the same row, near the water molecule, and between 0.14-0.21 Å measured from the bare Ti row. On the models with a single water molecule deposited on Ti we found migrations of up to 0.27 Å (0.27-0.25 Å water row, 0.18-0.20 Å bare row) on the perfect interface, up to 0.43 Å (0.26-0.28 Å water row; 0.43-0.36 Å bare row) on $TiO_{1.94}$-TiN and up to 0.29 Å (0.26-0.29 Å water row, 0.25-0.29 Å bare row) on $TiO_{1.88}$-TiN. The adsorption of 1 ML of water does not produce any extra distortions to the interfacial atoms.

The interface models show a distribution of reduced Ti^{3+} in TiO_2 that are mostly located near the oxide-nitride interface. We observe the presence of some Ti^{3+} on the rutile surface in TiO_2-TiN and $TiO_{1.94}$-TiN with 1/6 ML H_2O and at hydroxylated surfaces at coverages larger than 1/2ML. All the hydrated interfaces with Ti^{3+} on their surfaces correspond to the energetically unfavoured water adsorption modes on the surface, except for the $TiO_{1.94}$-TiN with 1/2 ML OH-H. However $TiO_{1.94}$-TiN is less stable compared to the ideal or the $TiO_{1.88}$-TiN interfaces. The adsorption of water leads to a similar number of localised Ti^{3+} for the 1/6 ML and 1 ML at the perfect interface compared to the bare surface with one less reduced Ti at 1/2 ML for the most stable water model. At the O/N exchanged interface, the amount of Ti^{3+} decreases progressively from 5 at the pristine surface, 4 on the 1/6 ML covered and 3 for higher surface coverages. The $TiO_{1.94}$-TiN interfaces presents 9 Ti^{3+} in all the interfaces except for the single OH-H, with 10 Ti^{3+}. The $TiO_{1.88}$-TiN interfaces presents 12 Ti^{3+} in all the interfaces except for half coverage, which has 14 Ti^{3+}. The variations in the apparent total number of reduced Ti^{3+} as a function of the water coverage are due to partial localization of electrons on Ti sites within the interface supercells.

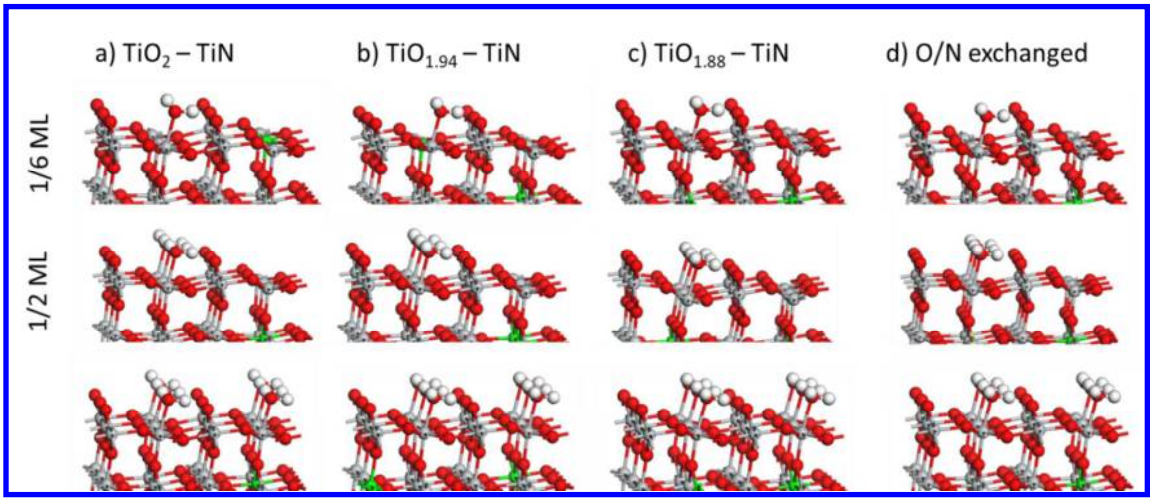

Figure 4. Structure of molecular water (H_2O) adsorbed at the rutile (110) surface on TiO_2 - TiN interfaces. Represented in columns from left to right are a) perfect TiO_2-TiN, b) O defective $TiO_{1.94}$-TiN, c) O defective $TiO_{1.88}$-TiN and d) O/N exchanged TiO_2-TiN interfaces. The rows from top to bottom are 1/6 ML (isolated water), 1/2 ML and 1 ML surface coverage

ratios. The Ti^{3+} atoms in TiO_2 are represented by green spheres, Ti^{4+} atoms in TiO_2 and all Ti in TiN are grey, N atoms are blue, O atoms are red and H atoms are white.

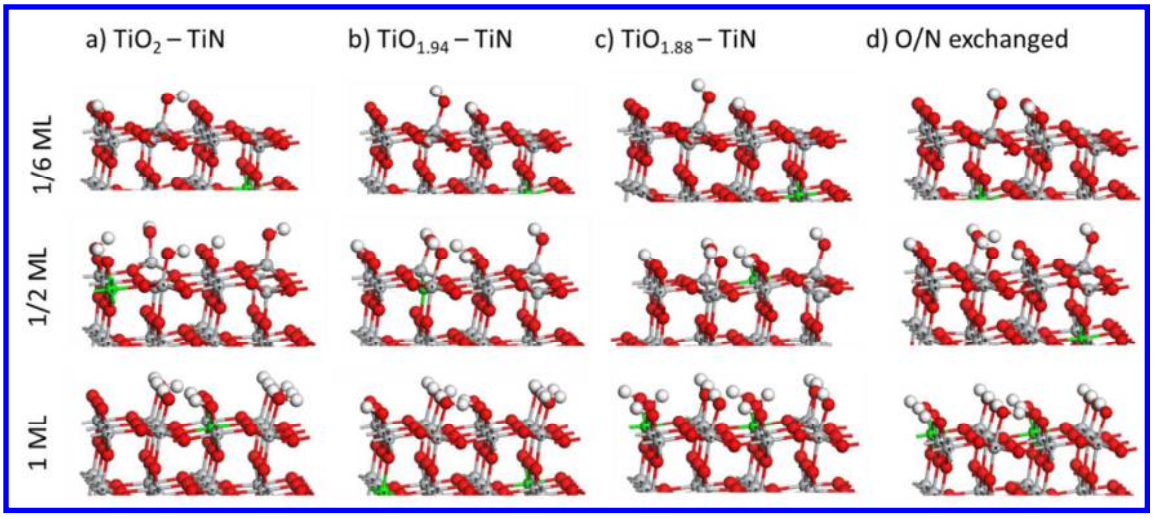

Figure 5. Structure of dissociated water (OH-H) adsorbed at the rutile (110) surface on TiO_2 -TiN interfaces. Represented in columns from left to right are a) perfect TiO_2-TiN, b) O defective $TiO_{1.94}$-TiN, c) O defective $TiO_{1.88}$-TiN and d) O/N exchanged TiO_2-TiN interfaces. The rows from top to bottom are for 1/6 ML (isolated water), 1/2 ML and 1 ML surface coverage ratios. The Ti^{3+} atoms in TiO_2 are represented by green spheres, Ti^{4+} atoms in TiO_2 and all Ti in TiN are grey, N atoms are blue, O atoms are red and H atoms are white.

Figure 6 shows the Electronic Density of States (EDOS) projected onto Ti 3d, N 2p and O 2p states for one isolated water adsorbed molecularly and dissociatively on the perfect TiO_2-TiN and $TiO_{1.88}$-TiN interfaces. The Ti^{3+} states lay in the gap between the highest occupied O 2p states in TiO_2 and the lowest unoccupied Ti 3d states in TiO_2. The TiN contribution to the EDOS presents metallic features, due to the contribution of Ti d-electrons. These features are common to all the interfaces and are not strongly affected by the adsorption of water. However, we observe clear differences in the EDOS between molecular and dissociative adsorption of water. Molecular water adsorbed on the perfect interface shows the O 2p states from water present in a broad band between 0.3 eV and 4.7 eV below the O 2p states from TiO_2 valence band, with main peaks around -1 eV and -4 eV measured from the top edge of the valence band. On the O defective interface, the O 2p states from water are between 0.1 eV and 4.8 eV below the O 2p from TiO_2 valence band, with main peaks around -1.5 eV and -4.5

eV measured from the valence band edge. When water is dissociatively adsorbed, O 2p states are more localized and exhibit more defined peaks that are shifted to lower energy states compared to the models with molecular water. The shift of O2p states from water towards lower energy indicates the higher stability of dissociative water adsorption compared to molecular adsorption at 1/6 ML coverage.

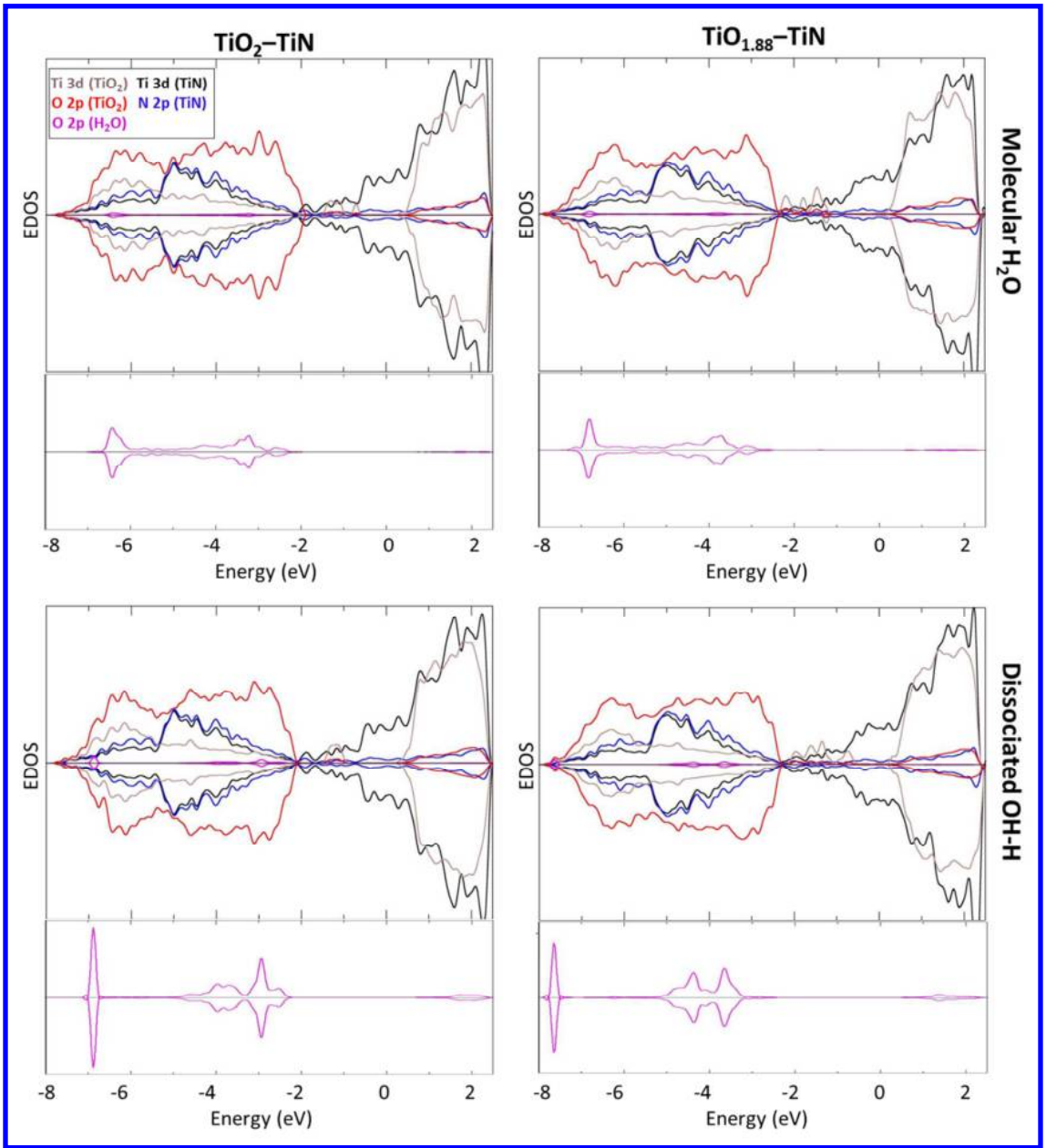

Figure 6. Spin polarized electronic Density of States (EDOS) of 1/6 ML covered TiO_2-TiN (left column) and $TiO_{1.88}$-TiN (right column) interfaces. The graphs on the top row represents the adsorption of molecular water and the bottom row stands for the dissociative adsorption mode. A legend with the contribution of each species is included in the top left graph. Ti 3d

electrons from TiN are represented with black lines, N 2p electrons in blue, Ti 3d electrons from TiO_2 in grey, O 2p electrons from TiO_2 in red and O 2p electrons from water in magenta. The individual contribution of O 2p states from water are shown under the main graphs and amplified by a factor of 23 with respect to the contribution of one single atom. The accumulated contribution of each species was taken into account for the total EDOS. The 0 eV energy stands for the Fermi level.

3.3 Thermodynamics of water adsorption at TiO_2-TiN

Having obtained the relevant TiN-TiO_2 structures with adsorbed water from 0 K DFT computations, we can now study the stability of each surface when in contact with an atmosphere containing a mixture of water vapour and oxygen. The key quantity of this study is the surface free energy defined as function of the chemical potential of O and H_2O, and the stable structures are those that minimize the surface free energy for a particular value of $\Delta\mu_O$ and $\Delta\mu_{H_2O}$.

Figure 7 shows the surface stability as a function of $\Delta\mu_O$ and $\Delta\mu_{H_2O}$, and these quantities are converted into a scale of partial pressure at two given temperatures T=300 K and T=1200 K using **Equation 5** and **Equation 6** in the Methodology Section. In **Figure 7** the range of $\Delta\mu_{H_2O}$ is from 0 eV to -3 eV. However to consider water vapor as a thermodynamically stable phase, the maximum value that $\Delta\mu_{H_2O}$ can assume is -0.91 eV, which corresponds to the chemical potential of water at the experimental critical point.[90]

Within this range we obtain five stable compositions under different environmental conditions:

a) the pristine TiO_2-TiN interface
b) the interface with 6 oxygen vacancies $TiO_{1.88}$-TiN with one dissociated water molecule (6V OH-H)
c) the interface with 6 oxygen vacancies $TiO_{1.88}$-TiN with half water monolayer of

coverage (6V $3H_2O$)

d) the perfect (defect-free) interface with one water monolayer ($6H_2O$)

e) the perfect interface with one dissociated water molecule (OH-H)

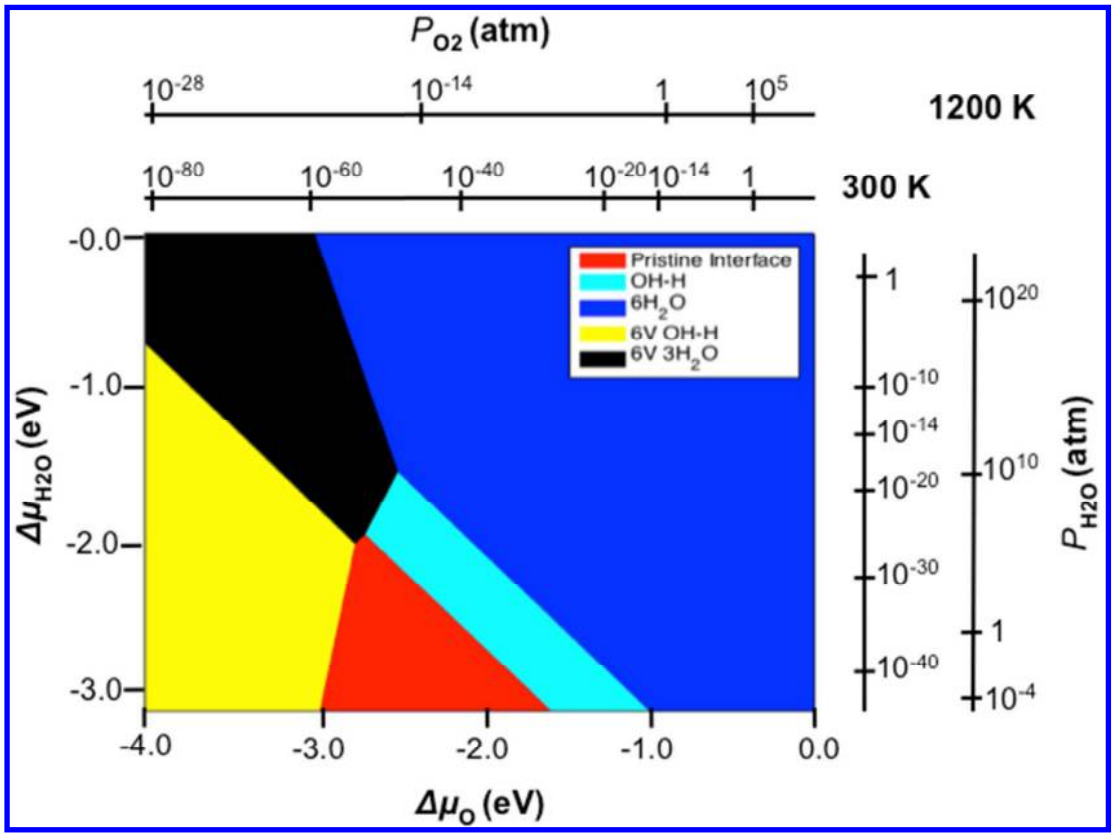

Figure 7. Surface phase diagram of stable structures of TiN-TiO_2 in equilibrium with a ''humid environment'', as a function of $\Delta\mu_{O_2}$ and $\Delta\mu_{H_2O}$ in the gas phase.

Some observations on the stability of water on TiO_2-TiN can be taken from the plot in Figure 7. At 300 K and high oxygen partial pressure (1atm), 1ML water coverage is always stable, independent of the water partial pressure, whereas at 300 K, to remove water we require low oxygen pressures of 10^{-14} atm, where we predict a transition to a 1/6 ML coverage of dissociated water at the interface; however this is seen only at very low water concentration. By increasing the temperature up to 1200 K and fixing P_{O2} to 10^{-10} atm, we observe two transitions. The first is a transition from a 1ML coverage of water coverage to dissociated water at 1/6 ML coverage and then complete desorption of water, but at very low water

pressures (P_{H2O}). From our analysis, oxygen vacancies are always stable in high concentration, however only at extremely low oxygen pressure, even at high T. However, this analysis assumes the vacancies form relative to a perfect oxide-nitride interface. In reality, vacancies can form and be trapped during oxide growth on the TiN surface.

If we compare the stability of selected interfaces, in order to resemble specific conditions, we observe from the phase diagrams that fully covered perfect and off-stoichiometric interfaces are always stable at ambient P_{H2O} and P_{O2} conditions. The phase diagrams for water surface coverage on the TiO_2-TiN, $TiO_{1.94}$-TiN, $TiO_{1.88}$-TiN and O/N exchanged systems are shown in **Figure S1**.

As a general trend, we can conclude that water is present at high coverage on TiO_2-TiN interfaces and dissociates only at very low P_{H2O}, with stabilisation of oxygen vacancies "clusters" at the condition of low oxygen pressures. The stability of a pristine interface is guaranteed only at very low pressure of both gases.

4. Conclusions

We presented a Density Functional Theory study with Hubbard +U correction on Ti 3d states (DFT+U) to describe the structural and electronic properties of molecular and dissociative adsorbed water at the rutile (110) surface of perfect and non-stoichiometric TiO_2-TiN interfaces. The surface free energy shows the perfect TiN-TiO_2 interface as the most stable at regular O pressures, while $TiO_{1.88}$–TiN is more favourable only at highly reducing conditions with $\Delta\mu_O < -3.15$ eV, although oxygen vacancies can be trapped during growth. The O/N exchanged interface is only ~0.01 eV/Å^2 higher relative to the perfect interface.

We discuss the stability of the molecular versus dissociated water adsorption modes as a function of the surface coverage and the nature of the TiO_2–TiN interface. The computed adsorption energies indicate that water is favourably adsorbed at the TiO_2–TiN interface. The

dissociative adsorption mode is more stable at low coverage (1/6 ML) at perfect and oxygen defective interfaces, which is in agreement with a previous study.[43] Our results show the that adsorption energy of the isolated OH-H is significantly stronger at the oxygen defective interfaces compared to the stoichiometric models, which is explained by the higher concentration of reduced Ti^{3+} in the oxide and the contribution of atomic relaxations within the TiO_{2-x}-TiN interfaces. Moving to higher coverages, we find that molecular adsorption is more stable than dissociative adsorption at 1/2 ML coverage on the perfect, O/N exchanged and $TiO_{1.88}$-TiN interfaces. The aligned H_2O distribution adsorption along [100] on the rutile surface is the most stable configuration due to the H bonds that are formed between adjacent molecules

Molecular adsorption is more stable on 1 ML covered perfect, O/N exchanged and $TiO_{1.88}$-TiN interfaces while at the $TiO_{1.94}$-TiN interface the molecular and mixed models are degenerate in energy. The decreasing binding energy per water at higher surface coverages is due to the energy required to drive surface and interfacial relaxations in the rutile-TiN system. On the TiO_2 surface, the Ti-O distances between surface Ti and O from H_2O increase upon adsorption of water. The Ti-O distances are larger on the molecularly covered surface than on hydroxylated. Surface Ti_{5f} atoms migrate up to 1 Å after binding with O on partially covered surfaces. Ab initio atomistic thermodynamics show that water is present at high coverage on all TiO_2-TiN interfaces and dissociates only at very low P_{H2O}. The pristine interface is only stable at very low pressure of O and H_2O.

These DFT+U simulations of water adsorbed on TiO_2–TiN (100) interface give a description of at the rutile TiO_2 (110) surface that grows on TiN in a realistic hydrated environment. The main outcomes of this study can be used for the further analysis of wettability or biomolecules adsorption on metal-oxides thin films.

Supporting Information

Surface phase diagrams for the relative water stability at selected TiN-TiO_2 structures in equilibrium within a humid environment.

Acknowledgements

This work was supported by the Environmental Protection Agency UisceSense project (W-2015-MS-21). The authors wish to acknowledge the DJEI/DES/SFI/HEA funded Irish Centre for High-End Computing (ICHEC) and the DECI-14 resource Bem based in Poland at WCSS with support from the PRACE aisbl for the provision of computational facilities and support.

References

(1) Zhang, S.; Zhu, W. TiN Coating of Tool Steels: a Review. *J. Mater. Process. Technol.* **1993,** *39*, 165-177.
(2) van Hove, R. P.; Sierevelt, I. N.; van Royen, B. J.; Nolte, P. A. Titanium-Nitride Coating of Orthopaedic Implants: a Review of the Literature. *BioMed Res. Int.* **2015**.
(3) Toth, L. *Transition metal carbides and nitrides*, Academic Press: **1971**.
(4) Pierson, H. O. *Handbook of Refractory Carbides & Nitrides: Properties, Characteristics, Processing and Apps*, William Andrew: 1996.
(5) Vaz, F.; Machado, P.; Rebouta, L.; Cerqueira, P.; Goudeau, P.; Rivière, J.; Alves, E.; Pischow, K.; De Rijk, J. Mechanical Characterization of Reactively Magnetron-Sputtered TiN Films. *Surf. Coat. Technol.* **2003,** *174*, 375-382.
(6) Johansson, L. I. Electronic and Structural Properties of Transition-Metal Carbide and Nitride Surfaces. *Surf. Sci. Rep.* **1995,** *21*, 177-250.
(7) Suni, I.; Sigurd, D.; Ho, K.; Nicolet, M. A. Thermal Oxidation of Reactively Sputtered Titanium Nitride and Hafnium Nitride Films. *J. Electrochem. Soc.* **1983,** *130*, 1210-1214.
(8) Desmaison, J.; Lefort, P.; Billy, M. Oxidation Mechanism of Titanium Nitride in Oxygen. *Oxid. Met.* **1979,** *13*, 505-517.
(9) Hou, X.; Chou, K. C.; Zhang, M. The Model for Oxidation Kinetics of Titanium Nitride Coatings. *Int. J. Appl. Ceram. Technol.* **2010,** *7*, 248-255.
(10) Wittmer, M.; Noser, J.; Melchior, H. Oxidation Kinetics of TiN Thin Films. *J Appl. Phys.* **1981,** *52*, 6659-6664.
(11) Moatti, A.; Bayati, R.; Narayan, J. Epitaxial Growth of Rutile TiO_2 Thin Films by Oxidation of TiN/Si{100} Heterostructure. *Acta Mater.* **2016,** *103*, 502-511.
(12) Ernsberger, C.; Nickerson, J.; Smith, T.; Miller, A.; Banks, D. Low Temperature Oxidation Behavior Of Reactively Sputtered TiN by X-ray Photoelectron Spectroscopy and Contact Resistance Measurements. *J. Vac, Sci. Technol., A: Vacuum, Surfaces, and Films* **1986,** *4*, 2784-2788.
(13) Rebouta, L.; Vaz, F.; Andritschky, M.; da Silva, M. F. Oxidation Resistance of (Ti,Al,Zr,Si)N Coatings in Air. *Surf. Coat. Technol.* **1995,** *76*, 70-74.
(14) Gwo, S.; Yeh, C.-L.; Chen, P.-F.; Chou, Y.-C.; Chen, T.; Chao, T.-S.; Hu, S.-F.; Huang, T.-Y. Local Electric-Field-Induced Oxidation of Titanium Nitride Films. *Appl. Phys. Lett.* **1999,** *74*, 1090-1092.
(15) Uetani, K.; Kajiyama, H.; Takagi, A.; Tokomoto, I.; Koizumi, Y.; Nose, K.; Ihara, Y.; Kato, A.; Onisawa, K.-i.; Minemura, T. Oxidation Mechanism of Ultra Thin TiN Films Prepared by an Advanced Ion-Plating Method. *Mater. Trans.* **2001,** *42*, 403-406.

(16) Di Valentin, C.; Finazzi, E.; Pacchioni, G.; Selloni, A.; Livraghi, S.; Paganini, M. C.; Giamello, E. N-doped TiO_2: Theory and Experiment. *Chem. Phys.* **2007,** *339*, 44-56.
(17) Xie, Z.; Liu, X.; Zhan, P.; Wang, W.; Zhang, Z. Tuning the Optical Bandgap of TiO_2-Tin Composite Films as Photocatalyst in the Visible Light. *AIP Adv.* **2013,** *3*, 062129.
(18) Morikawa, T.; Asahi, R.; Ohwaki, T.; Aoki, K.; Taga, Y. Band-Gap Narrowing of Titanium Dioxide by Nitrogen Doping. *Jpn. J. Appl. Phys.* **2001,** *40*, L561.
(19) Zimmermann, J.; Finnis, M. W.; Ciacchi, L. C. Vacancy Segregation in the Initial Oxidation Stages of the TiN(100) Surface. *J. Chem. Phys.* **2009,** *130*, 134714.
(20) Gutiérrez Moreno, J. J.; Nolan, M. Ab Initio Study of the Atomic Level Structure of the Rutile TiO_2(110)–Titanium Nitride (TiN) Interface. *ACS Appl. Mat. Interfaces* **2017,** *9*, 38089-38100.
(21) Diebold, U. The Surface Science of Titanium Dioxide. *Surf. Sci. Rep.* **2003,** *48*, 53-229.
(22) Cui, C.; Liu, H.; Li, Y.; Sun, J.; Wang, R.; Liu, S.; Greer, A. L. Fabrication and Biocompatibility of Nano-TiO_2/Titanium Alloys Biomaterials. *Mat. Lett.* **2005,** *59*, 3144-3148.
(23) Bao, S. J.; Li, C. M.; Zang, J. F.; Cui, X. Q.; Qiao, Y.; Guo, J. New Nanostructured TiO_2 for Direct Electrochemistry and Glucose Sensor Applications. *Adv. Funct. Mat.* **2008,** *18*, 591-599.
(24) Lin, H.-M.; Keng, C.-H.; Tung, C.-Y. Gas-Sensing Properties of Nanocrystalline TiO_2. *Nanostruct. Mat.* **1997,** *9*, 747-750.
(25) Pan, J.; Leygraf, C.; Thierry, D.; Ektessabi, A. Corrosion Resistance for Biomaterial Applications of TiO_2 Films Deposited on Titanium and Stainless Steel by Ion-Beam-Assisted Sputtering. *J Biomed. Mat. Res. Part A* **1997,** *35*, 309-318.
(26) Hashimoto, K.; Irie, H.; Fujishima, A. TiO_2 Photocatalysis: a Historical Overview and Future Prospects. *Jpn. J. Appl. Phys.* **2005,** *44*, 8269.
(27) Tang, J.; Durrant, J. R.; Klug, D. R. Mechanism of Photocatalytic Water Splitting in TiO_2. Reaction of Water with Photoholes, Importance of Charge Carrier Dynamics, and Evidence for Four-Hole Chemistry. *J. Am. Chem. Soc.* **2008,** *130*, 13885-13891.
(28) Geetha, M.; Singh, A.; Asokamani, R.; Gogia, A. Ti Based Biomaterials, the Ultimate Choice for Orthopaedic Implants–a Review. *Prog. Mat. Sci.* **2009,** *54*, 397-425.
(29) Fuerte, A.; Hernández-Alonso, M.; Maira, A.; Martinez-Arias, A.; Fernandez-Garcia, M.; Conesa, J.; Soria, J. Visible Light-Activated Nanosized Doped-TiO_2 photocatalysts. *Chem. Commun.* **2001**, 2718-2719.
(30) Park, H.; Park, Y.; Kim, W.; Choi, W. Surface Modification of TiO_2 Photocatalyst for Environmental Applications. *J. Photochem. Photobiol., B: Photochem. Rev.* **2013,** *15*, 1-20.
(31) Niinomi, M. Mechanical Biocompatibilities of Titanium Alloys for Biomedical applications. *J. Mech. Behav. Biomed. Mat.* **2008,** *1*, 30-42.
(32) Niinomi, M. Recent Metallic Materials for Biomedical Applications. *Metall. Mater. Trans. A* **2002,** *33*, 477-486.
(33) Graziani, L.; Quagliarini, E.; Bondioli, F.; D'Orazio, M. Durability of Self-Cleaning TiO_2 Coatings on Fired Clay Brick Façades: Effects of UV Exposure and Wet & Dry Cycles. *Building Environm.* **2014,** *71*, 193-203.
(34) Graziani, L.; Quagliarini, E.; Osimani, A.; Aquilanti, L.; Clementi, F.; Yéprémian, C.; Lariccia, V.; Amoroso, S.; D'Orazio, M. Evaluation of Inhibitory Effect of TiO_2 Nanocoatings Against Microalgal Growth on Clay Brick Façades Under Weak UV Exposure Conditions. *Building Environm.* **2013,** *64*, 38-45.
(35) Lorenzetti, M.; Bernardini, G.; Luxbacher, T.; Santucci, A.; Kobe, S.; Novak, S. Surface Properties of Nanocrystalline TiO_2 Coatings in Relation to the In Vitro Plasma Protein Adsorption. *Biomed. Mater.* **2015,** *10*, 045012.

(36) Wang, R.; Hashimoto, K.; Fujishima, A.; Chikuni, M.; Kojima, E.; Kitamura, A.; Shimohigoshi, M.; Watanabe, T. Photogeneration of Highly Amphiphilic TiO_2 Surfaces. *Adv. Mat.* **1998,** *10*, 135-138.
(37) Hugenschmidt, M. B.; Gamble, L.; Campbell, C. T. The Interaction of H_2O with a TiO_2 (110) Surface. *Surf. Sci.* **1994,** *302*, 329-340.
(38) Henderson, M. A. The Interaction of Water with Solid Surfaces: Fundamental Aspects Revisited. *Surf. Sci. Rep.* **2002,** *46*, 1-308.
(39) Pan, J. M.; Maschhoff, B.; Diebold, U.; Madey, T. Interaction of Water, Oxygen, and Hydrogen with TiO_2 (110) Surfaces Having Different Defect Densities. *J. Vac. Sci. Technol., A* **1992,** *10*, 2470-2476.
(40) Lee, S.-Y.; Park, S.-J. TiO_2 Photocatalyst for Water Treatment Applications. *J. Ind. Eng. Chem.* **2013,** *19*, 1761-1769.
(41) Kumar, N.; Kent, P. R.; Wesolowski, D. J.; Kubicki, J. D. Modeling Water Adsorption on Rutile (110) Using van der Waals Density Functional and DFT+ U Methods. *J. Phys. Chem. C* **2013,** *117*, 23638-23644.
(42) Schaub, R.; Thostrup, P.; Lopez, N.; Lægsgaard, E.; Stensgaard, I.; Nørskov, J. K.; Besenbacher, F. Oxygen Vacancies as Active Sites for Water Dissociation on Rutile TiO_2 (110). *Phys. Rev. Lett.* **2001,** *87*, 266104.
(43) Kowalski, P. M.; Meyer, B.; Marx, D. Composition, structure, and stability of the rutile TiO_2 (110) surface: Oxygen Depletion, Hydroxylation, Hydrogen Migration, and Water Adsorption. *Phys. Rev. B* **2009,** *79*, 115410.
(44) Patsalas, P.; Kalfagiannis, N.; Kassavetis, S.; Abadias, G.; Bellas, D.; Lekka, C.; Lidorikis, E. Conductive nitrides: Growth Principles, Optical and Electronic Properties, and their Perspectives in Photonics and Plasmonics. *Mat. Sci. Eng. R: Reports* **2018,** *123*, 1-55.
(45) Oh, U. C.; Je, J. H. Effects of Strain Energy on the Preferred Orientation of TiN Thin Films. *J. Appl. Phys.* **1993,** *74*, 1692-1696.
(46) Ikeda, S.; Palleau, J.; Torres, J.; Chenevier, B.; Bourhila, N.; Madar, R. Film Texture Evolution in Plasma Treated TiN thin Films. *J. Appl. Phys.* **1999,** *86*, 2300-2306.
(47) Ponon, N. K.; Appleby, D. J. R.; Arac, E.; King, P. J.; Ganti, S.; Kwa, K. S. K.; O'Neill, A. Effect of Deposition Conditions and Post Deposition Anneal on Reactively Sputtered Titanium Nitride Thin Films. *Thin Solid Films* **2015,** *578*, 31-37.
(48) Jung, J.; Shin, H.-J.; Kim, Y.; Kawai, M. Controlling Water Dissociation on an Ultrathin MgO Film by Tuning Film Thickness. *Phys. Rev. B* **2010,** *82*, 085413.
(49) Shin, H.-J.; Jung, J.; Motobayashi, K.; Yanagisawa, S.; Morikawa, Y.; Kim, Y.; Kawai, M. State-Selective Dissociation of a Single Water Molecule on an Ultrathin MgO Film. *Nature Mat.* **2010,** *9*, 442.
(50) Song, Z.; Fan, J.; Xu, H. Strain-Induced Water Dissociation on Supported Ultrathin Oxide Films. *Sci. Rep.* **2016,** *6*, 22853.
(51) Seifitokaldani, A.; Savadogo, O.; Perrier, M. Density functional theory (DFT) Computation of The Oxygen Reduction Reaction (ORR) on Titanium Nitride (TiN) Surface. *Electrochim. Acta* **2014,** *141*, 25-32.
(52) Marlo, M; Milman, V. Density-Functional Study of Bulk and Surface Properties of Titanium Nitride using Different Exchange-Correlation Functionals. *Phys. Rev. B* **2000,** *62*, 2899-2907.
(53) Perron, H.; Domain, C.; Roques, J.; Drot, R.; Simoni, E.; Catalette, H. Optimisation of Accurate Rutile TiO_2 (110), (100), (101) and (001) Surface Models from Periodic DFT Calculations. *Theor. Chem. Acc.* **2007,** *117*, 565-574.
(54) Reuter, K.; Scheffler, M. Composition, Structure, and Stability of RuO_2 (110) as a Function of Oxygen Pressure. *Phys. Rev. B* **2001,** *65*, 035406.

(55) Hafner, J. Ab□Initio Simulations of Materials Using VASP: Density Functional Theory and Beyond. *J. Comp. Chem.* **2008,** *29*, 2044-2078.
(56) Blöchl, P. E. Projector Augmented-Wave Method. *Phys. Rev. B* **1994,** *50*, 17953-17979.
(57) Kresse, G.; Joubert, D. From Ultrasoft Pseudopotentials to the Projector Augmented-Wave Method. *Phys. Rev. B* **1999,** *59*, 1758-1775.
(58) Perdew, J. P.; Wang, Y. Accurate and Simple Analytic Representation of the Electron-Gas Correlation Energy. *Phys. Rev. B* **1992,** *45*, 13244-13249.
(59) Morgan, B. J.; Watson, G. W. A DFT + U Description of Oxygen Vacancies at the TiO_2 Rutile (110) Surface. *Surf. Sci.* **2007,** *601*, 5034-5041.
(60) Arroyo-de Dompablo, M.; Morales-García, A.; Taravillo, M. DFT+ U Calculations of Crystal Lattice, Electronic Structure and Phase Stability Under Pressure of TiO_2 Polymorphs. *J. Chem. Phys.* **2011,** *135*, 054503.
(61) Himmetoglu, B.; Floris, A.; Gironcoli, S.; Cococcioni, M. Hubbard-Corrected DFT Energy Functionals: The LDA+U Description of Correlated Systems. *Int. J. Quantum Chem.* **2014,** *114*, 14-49.
(62) Iwaszuk, A.; Nolan, M. Reactivity of sub 1 nm Supported Clusters:$(TiO_2)_n$ Clusters Supported on Rutile TiO_2 (110). *Phys. Chem. Chem. Phys.* **2011,** *13*, 4963-4973.
(63) Graciani, J.; Plata, J. J.; Sanz, J. F.; Liu, P.; Rodriguez, J. A. A Theoretical Insight into the Catalytic Effect of a Mixed-Metal Oxide at the Nanometer Level: The Case of the Highly Active Metal/CeO_x/TiO_2 (110) Catalysts. *J. Chem. Phys.* **2010,** *132*, 104703.
(64) Cheng, H.; Selloni, A. Energetics and Diffusion of Intrinsic Surface and Subsurface Defects on Anatase TiO_2 (101). *J Chem. Phys.* **2009,** *131*, 054703.
(65) Tang, W.; Sanville, E.; Henkelman, G. A Grid-Based Bader Analysis Algorithm Without Lattice Bias. *J. Phys: Condens. Matter* **2009,** *21*, 084204.
(66) Hegde, R. I.; Fiordalice, R. W.; Travis, E. O.; Tobin, P. J. Thin Film Properties of Low□Pressure Chemical Vapor Deposition Tin Barrier For Ultra-Large-Scale Integration Applications. *J. Vac. Sci. Technol., B* **1993,** *11*, 1287-1296.
(67) Gutiérrez Moreno, J. J. DOI: http://dx.doi.org/10.17172/NOMAD/2017.09.22-1.
(68) Saqlain, M. A., Hussain, A., Siddiq, M., Leitão, A. A. Water Dissociation and CO Oxidation over Au/Anatase Catalyst. A DFT-D2 Study. *Appl. Surf. Sci.* ***2018,*** *435*, 1168-1173.
(69) Kumar, N., Kent, P. R., Wesolowski, D. J., Kubicki, J. D. Modeling Water Adsorption on Rutile (110) Using van der Waals Density Functional and DFT+ U Methods. *J. Phys. Chem. C*, **2013**, *117,* 23638-23644.
(70) Fernández-Torre, D., Kośmider, K., Carrasco, J., Ganduglia-Pirovano, M. V., Pérez, R. Insight into the Adsorption of Water on the Clean CeO_2 (111) Surface with van der Waals and Hybrid Density Functionals. *J. Phys. Chem. C*, **2012**, *116*, 13584-13593.
(71) Stull, D. R.; Prophet, H. *JANAF Thermochemical Tables*; DTIC Document: 1971.
(72) Fronzi, M.; Piccinin, S.; Delley, B.; Traversa, E.; Stampfl, C. Water Adsorption on the Stoichiometric and Reduced CeO_2 (111) Surface: a First-Principles Investigation. *Phys. Chem. Chem. Phys.* **2009,** *11*, 9188-9199.
(73) Fronzi, M.; Piccinin, S.; Delley, B.; Traversa, E.; Stampfl, C. CH_x Adsorption (x=1-4) and Thermodynamic Stability on the CeO_2 (111) Surface: a First-Principles Investigation. *RSC Adv.* **2014,** *4*, 12245-12251.
(74) Fronzi, M.; Soon, A.; Delley, B.; Traversa, E.; Stampfl, C. Stability and Morphology of Cerium Oxide Surfaces in an Oxidizing Environment: a First-Principles Investigation. *J. Chem. Phys.* **2009,** *131*, 104701.
(75) Straumanis, M.; Ejima, T.; James, W. The TiO_2 Phase Explored by the Lattice Constant and Density Method. *Acta Crystallogr.* **1961,** *14*, 493-497.

(76) Schönberg, N.; Overend, W.; Munthe-Kaas, A.; Sörensen, N. A. An X-ray Study of the Tantalum-Nitrogen System. *Acta Chem. Scand.* **1954,** *8*, 199-203.
(77) Pan, X.; Yang, M.-Q.; Fu, X.; Zhang, N.; Xu, Y.-J. Defective TiO_2 with Oxygen Vacancies: Synthesis, Properties and Photocatalytic Applications. *Nanoscale* **2013,** *5*, 3601-3614.
(78) Tilocca, A.; Di Valentin, C.; Selloni, A. O_2 Interaction and Reactivity on a Model Hydroxylated Rutile (110) Surface. *J. Phys. Chem. B* **2005,** *109,* 20963-20967.
(79) Wendt, S.; Matthiesen, J.; Schaub, R.; Vestergaard, E. K.; Lægsgaard, E.; Besenbacher, F.; Hammer, B. Formation and Splitting of Paired Hydroxyl Groups on Reduced TiO_2 (110). *Phys. Rev. Lett.* **2006,** *96*, 066107.
(80) Wendt, S.; Schaub, R.; Matthiesen, J.; Vestergaard, E. K.; Wahlström, E.; Rasmussen, M. D.; Thostrup, P.; Molina, L.; Lægsgaard, E.; Stensgaard, I. Oxygen Vacancies on TiO_2 (110) and their Interaction with H_2O and O_2: A Combined High-Resolution STM and DFT study. *Surf. Sci.* **2005,** *598*, 226-245.
(81) Carrasco, J.; López□Durán, D.; Liu, Z.; Duchoň, T.; Evans, J.; Senanayake, S. D.; Crumlin, E. J.; Matolín, V.; Rodríguez, J. A.; Ganduglia□Pirovano, M. V. In Situ and Theoretical Studies for the Dissociation of Water on an Active Ni/CeO_2 Catalyst: Importance of Strong Metal–Support Interactions for the Cleavage of O–H Bonds. *Angew. Chem. Int. Ed.* **2015,** *54*, 3917-3921.
(82) Mullins, D. R.; Albrecht, P. M.; Chen, T.-L.; Calaza, F. C.; Biegalski, M. D.; Christen, H. M.; Overbury, S. H. Water Dissociation on CeO_2 (100) and CeO_2 (111) Thin Films. *J. Phys. Chem. C* **2012,** *116* (36), 19419-19428.
(83) Deng, X.; Herranz, T.; Weis, C.; Bluhm, H.; Salmeron, M. Adsorption of Water on Cu_2O and Al_2O_3 Thin Films. *J. Phys. Chem. C* **2008,** *112*, 9668-9672.
(84) Harris, L. A.; Quong, A. A. Molecular Chemisorption as the Theoretically Preferred Pathway for Water Adsorption on Ideal Rutile TiO_2 (110). *Phys. Rev. Lett.* **2004,** *93*, 086105.
(85) Perron, H.; Vandenborre, J.; Domain, C.; Drot, R.; Roques, J.; Simoni, E.; Ehrhardt, J.-J.; Catalette, H. Combined Investigation of Water Sorption on TiO_2 Rutile (110) Single Crystal Face: XPS vs. Periodic DFT. *Surf. Sci.* **2007,** *601*, 518-527.
(86) Brinkley, D., Dietrich, M., Engel, T., Farrall, P., Gantner, G., Schafer, A., Szuchmacher, A. A Modulated Molecular Beam Study of the Extent of H_2O Dissociation on TiO_2 (110). *Surf. Sci.* **1998**, *395*, 292-306.
(87) Hugenschmidt, M. B., Gamble, L., Campbell, C. T. The Interaction of H_2O with a TiO_2 (110) Surface. *Surf. Sci.*, **1994**, *302*, 329-340.
(88) Henderson, M. A. An HREELS and TPD Study of Water on TiO_2 (110): The Extent of Molecular Versus Dissociative Adsorption. *Surf. Sci.* **1996**, *355*, 151-166.
(89) Lee, H. Y.; Park, Y. H.; Ko, K. H. Correlation between Surface Morphology and Hydrophilic/Hydrophobic Conversion of MOCVD−TiO_2 Films. *Langmuir* **2000,** *16*, 7289-7293.
(90) Sun, Q.; Reuter, K.; Scheffler, M. Effect of a Humid Environment on the Surface Structure of RuO_2 (110). *Phys. Rev. B* **2003,** *67*, 205424.

TOC

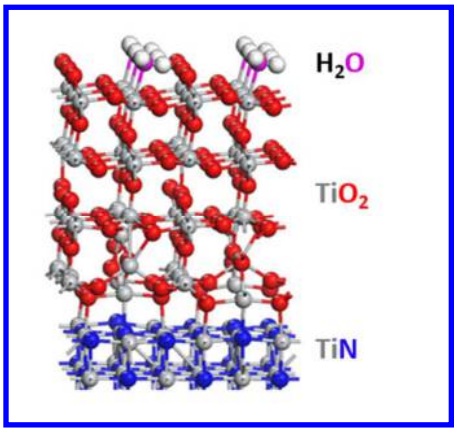

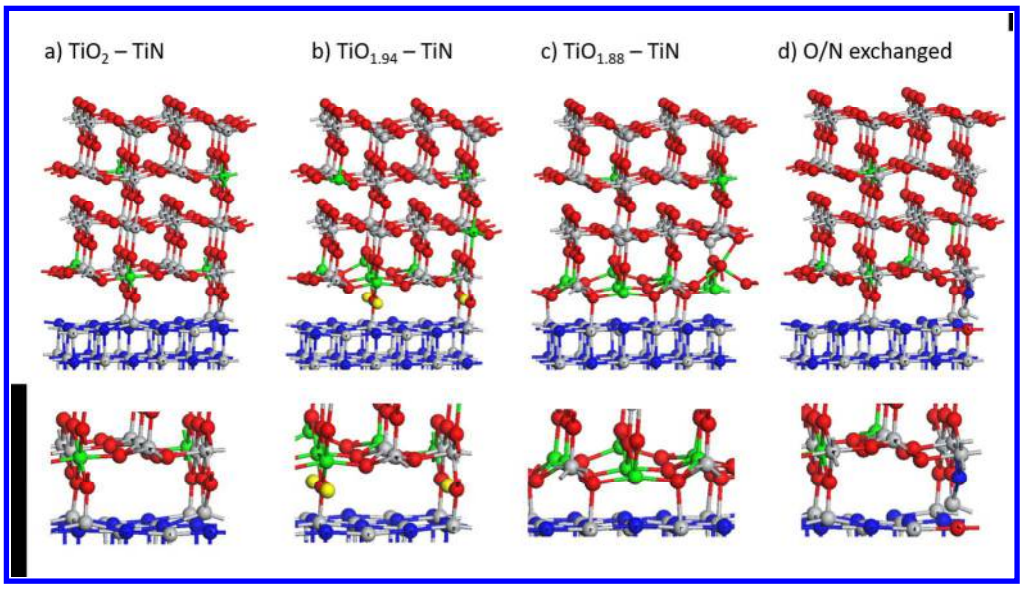

Figure 1

266x150mm (150 x 150 DPI)

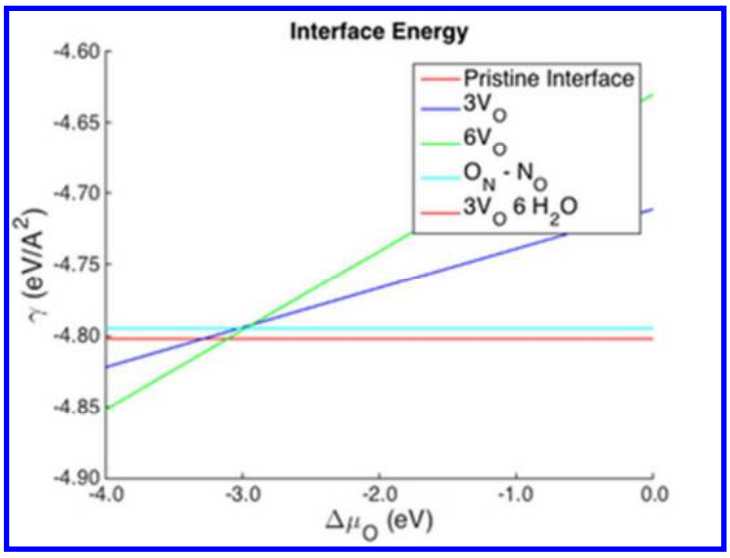

Figure 2

29x22mm (300 x 300 DPI)

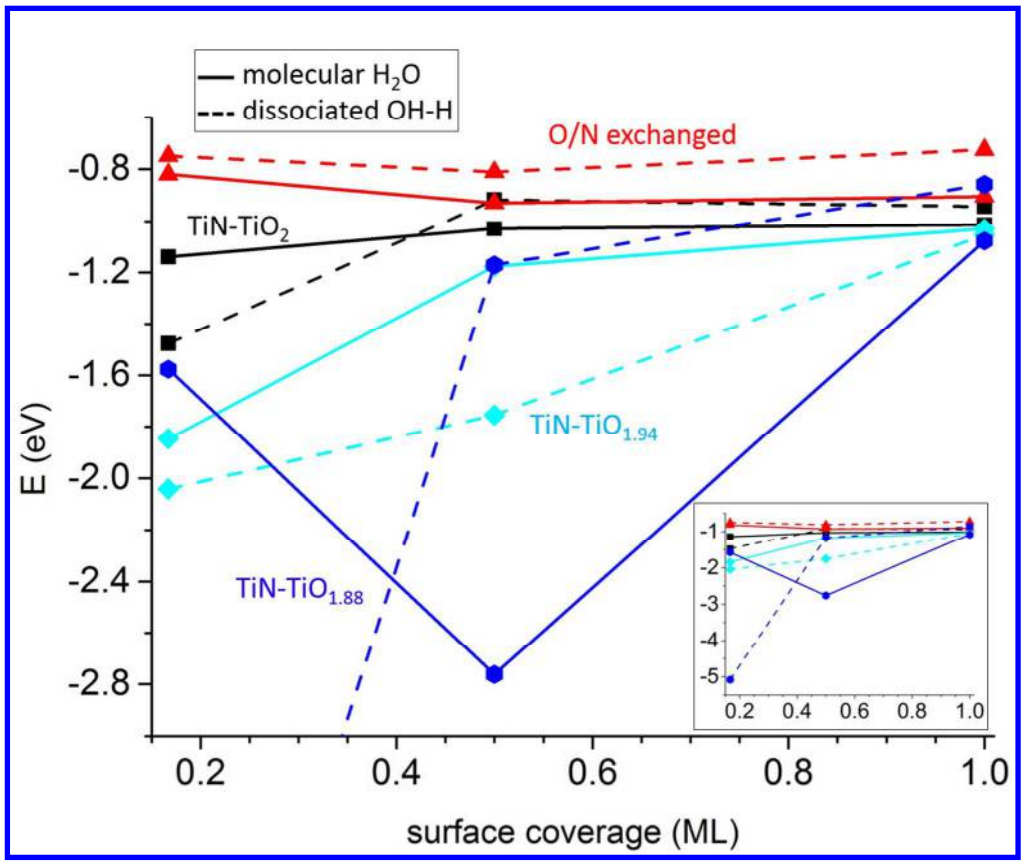

Figure 3

233x196mm (150 x 150 DPI)

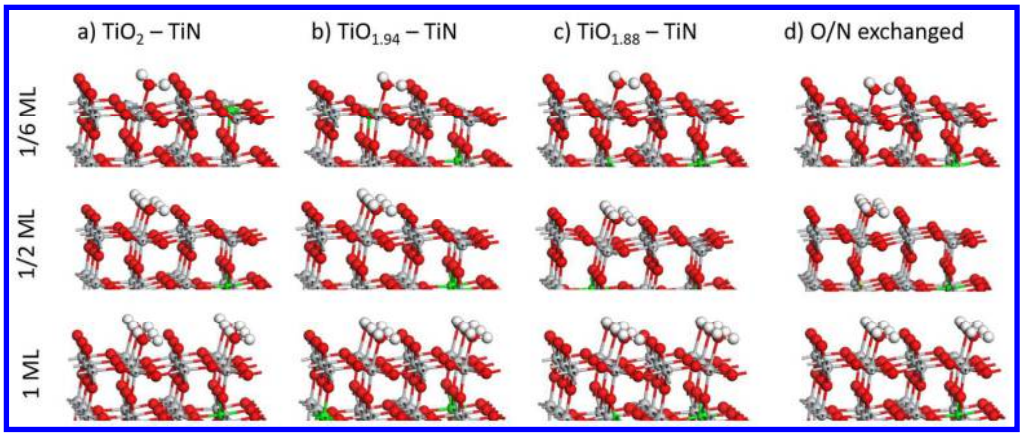

Figure 4

258x106mm (150 x 150 DPI)

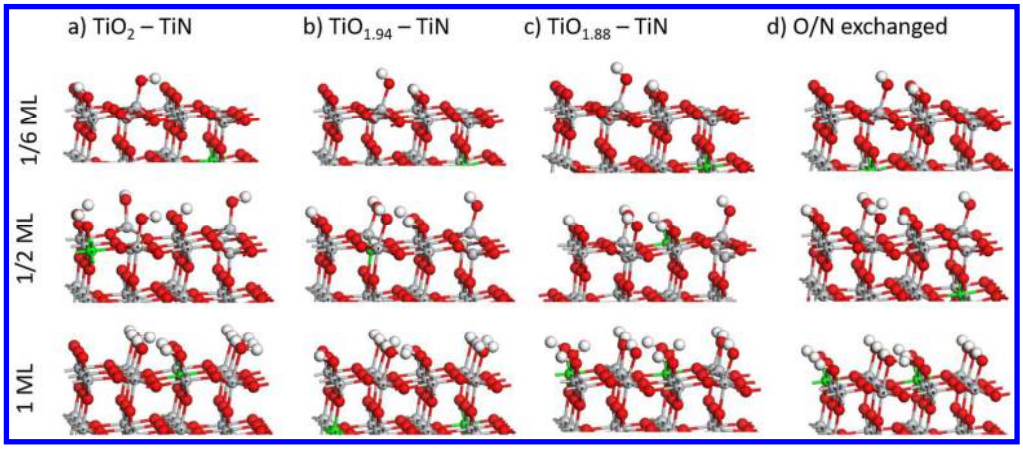

Figure 5

256x109mm (150 x 150 DPI)

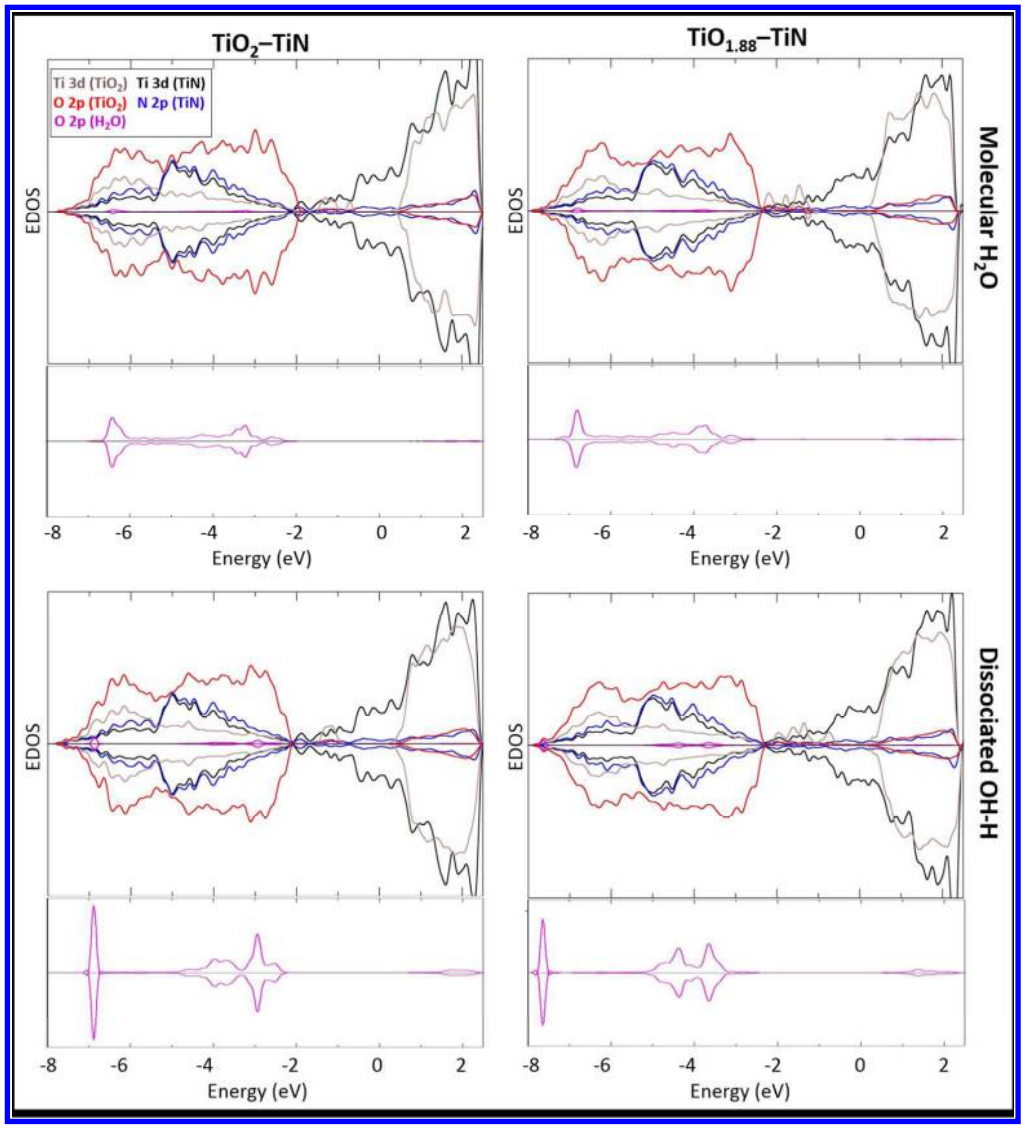

Figure 6

263x290mm (150 x 150 DPI)

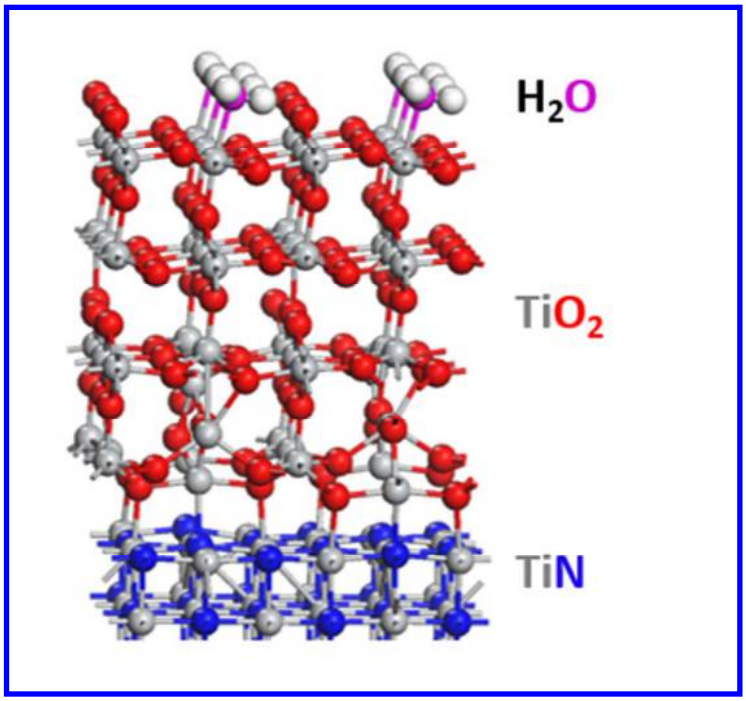

TOC

61x57mm (150 x 150 DPI)